2016-01-01

Analysis of Road Vehicle Aerodynamics with Computational Fluid Dynamics

Christian Armando Mata
University of Texas at El Paso, camata@miners.utep.edu

ANALYSIS OF ROAD VEHICLE AERODYNAMICS WITH COMPUTATIONAL FLUID DYNAMICS

CHRISTIAN ARMANDO MATA

Master's Program in Mechanical Engineering

APPROVED:

Jack Chessa, Ph.D., Chair

Norman D Love, Ph.D.

Bill Tseng, Ph.D.

Charles Ambler, Ph.D.
Interim Dean of the Graduate School

Dedication

I would like to dedicate this work, to my mother, father, and brother. With their support and the support of my loved ones, that make this possible. Thank you for all you have given me, and for always being there for me.

ANALYSIS OF ROAD VEHICLE AERODYNAMICS WITH COMPUTATIONAL FLUID DYNAMICS

by

CHRISTIAN ARMANDO MATA, B.S.

THESIS

Presented to the Faculty of the Graduate School of

The University of Texas at El Paso

in Partial Fulfillment

of the Requirements

for the Degree of

MASTER OF SCIENCE

Department of Mechanical Engineering

THE UNIVERSITY OF TEXAS AT EL PASO

May 2016

Acknowledgements

I would like to thank my graduate advisor Dr. Jack Chessa. Your guidance and assistance have made this possible. I would also like to thank Cyrus Proctor who is part of the support team from the Texas Advanced Computing Center (TACC). Finally, Special thanks to Abigail Arrington, Shannon Earls, and Michael Barton, from Altair-Hyperworks.

Table of Contents

List of Tables

List of Figures

List of Illustrations

Chapter 1: Background and Theory

1.1 Introduction

The aerodynamics of a vehicle influence many aspects of its performance, which is why the importance of a well optimized aerodynamic design is a major area of focus in modern vehicles. With today's increasing focus on energy and sustainability there is a larger push for increasingly fuel efficient and technologically advanced vehicles which have less of an environmental effect. There are many emerging technologies which have improved fuel efficiency and decreased our consumption of fossil fuels. This can include biofuels, hybrid technologies, as well as full electric vehicles. However regardless of the type of fuel being consumed, aerodynamics can have a significant effect on the vehicles fuel consumption.

By designing road vehicles with a well optimized aerodynamic body, it is possible to improve fuel efficiency, vehicle handling, as well as top velocity. However, the limitations of vehicle appearance and cosmetics, as well as general geometry and passenger comforts present several challenges when optimizing a vehicles aerodynamic design.

1.2 Shell Eco Marathon

With the recent demands for higher fuel efficiency in consumer vehicles, the Shell oil company, promotes engineering innovation in the form of a competition. The Shell Eco-Marathon is an international competition which focuses on encouraging students to design and innovate prototype vehicles to achieve high levels of fuel efficiency [1]. The competition focuses on the design of two main types of vehicles, taking advantage of 6 different types of fuels and power sources. The two main types of vehicles include a prototype category which has minimum regulation in order to achieve the highest possible fuel efficiency with little limitations [1]. The other is referred to as the Urban Concept category, where vehicles are designed in a more traditional manner, and vehicles are required to have a more street legal design that includes

headlights, tail lights, and doors. For this study the main focus of the vehicle design will be on a prototype category vehicle design [1].

1.3 Effects on Vehicle Performance

Achieving high fuel efficiency requires a large amount of optimization on several aspects of a vehicles design. The main components which affect a vehicles fuel efficiency directly are the Engine efficiency, the vehicle weight, the amount of frictional losses, as well as the aerodynamics of the vehicle. While the engine efficiency has a major role in the fuel consumption, other aspects such as the vehicles mass and frictional losses with in the wheels or drivetrain can have a significant influence as well. The effects of aerodynamics on fuel efficiency, are more related to the vehicles velocity. While a vehicle can have minimal drag at a cruising speed, the force can become more substantial as the same vehicle approaches high way speed. A vehicle with a low drag force not only becomes more fuel efficient, it can also take advantage of requiring less power to propel forward at a higher speed [2].

The effects of aerodynamics on vehicle performance are influenced by two major components. These include the drag force and the lift force, which are caused due to the external flow of the fluid flowing over the vehicles geometry. A vehicles drag force causes an increase in resistance to forward momentum, and thus has a major contribution to the fuel efficiency, as well as the acceleration and top speed of a vehicle. On the other hand, a lift force can be caused due to large amounts of pressure beneath the vehicles body, which can affect the vehicles handling and traction.

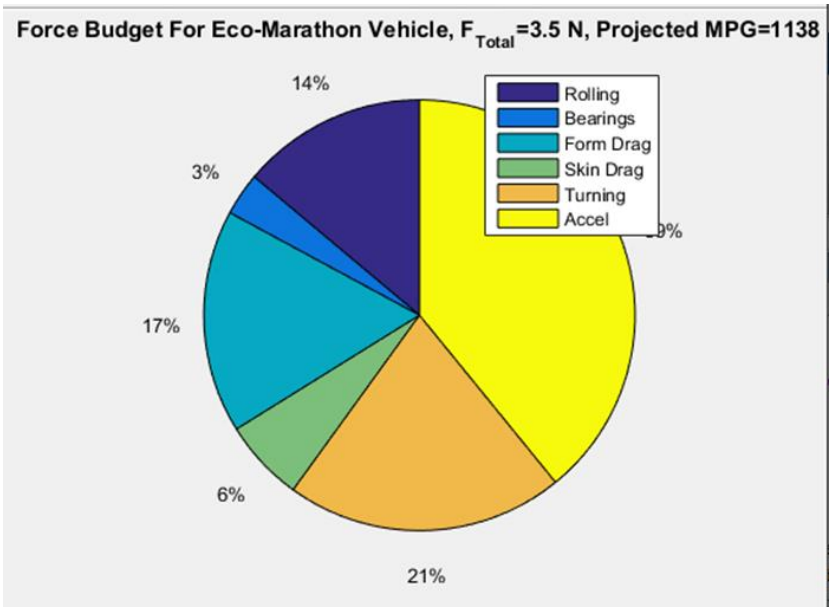

Figure 1.1: Pie graph generated by matlab code

Using a code generated on matlab shown in the appendix, a force budget is calculated to show the maximum amount of drag force required to achieve a high mileage. The graph shown in figure 1.1 is generated by this code and shows the influence of each type of loss on the vehicle to achieve 1,100 miles per gallon. From this calculation the total amount of losses is about $F_{total} = 3.5N$. Where the aerodynamic drag accounts to 23% of this total amount. This shows how the aerodynamic drag can have a substantial effect on the vehicles mileage despite the low forces acting on the vehicle.

1.4 Background Theory

The combination of pressure forces as well as tangential shear forces compose the drag forces excreted on a body. As explained by Cengel, in two dimensional flow the differential drag force dF which is acting on a differential area dA, is dependent on the pressure force PdA and the shear force τdA [2]. Where depending on the angle θ measured from the normal in which the flow approaches the surface, the drag force can be calculated at any given point with equation 1 and equation 2 [2]:

$$dF_d = -PdAcos\theta + \tau dA \quad \text{(eq. 1)}$$

$$dF_l = -PdAcos\theta - \tau dA \quad \text{(eq.2)}$$

This applies as well to the lift force on a body, however the direction of the shear forces changes. When focusing on the entire surface area of the body A, the equations then become:

$$F_d = \int_A dF_d = \int_A (-P\cos\theta + \tau\sin\theta)\, dA \quad \text{(eq. 3)}$$

$$F_l = \int_A dF_l = \int_A (-P\cos\theta - \tau\sin\theta)\, dA \quad \text{(eq.4)}$$

However, these equations are used mostly in computational methods. When working with the drag of an object there is a large dependence on the density and velocity of the fluid. In order to utilize non dimentionalized values such as drag and lift coefficients, the equation can be written in a more practical form with respect to its dynamic pressure [2]. This will result in the equations [2]:

$$F_d = \frac{1}{2}\rho V^2 A C_d \quad \text{(eq.5)}$$

$$F_l = \frac{1}{2}\rho V^2 A C_l \quad \text{(eq.6)}$$

In many cases the drag and lift coefficients or the drag and lift forces are unknown. This issue can be resolved by either using known documented values for these coefficient, or measuring the drag force or lift force of the object in order to calculate this equation.

As the fluid approaches the surface the velocity of the fluid approaches stagnation. The region in which there is a variation in velocity is called the boundary layer [2]. This layer is related to the Reynolds number and increases along the length of the surface in the x direction. The Reynolds number is then written as:

$$Re_x = \frac{\rho V x}{\mu} = \frac{Vx}{\nu} \quad \text{(eq.7)}$$

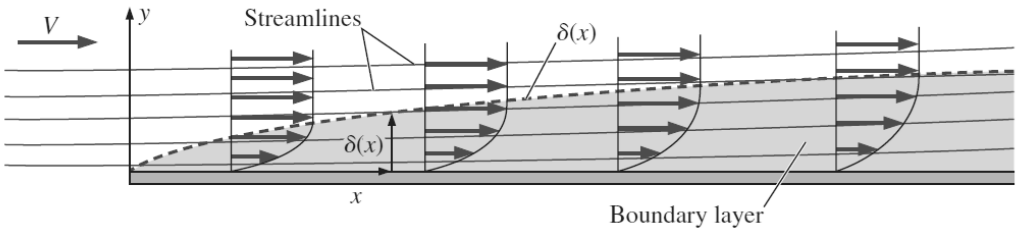

Figure 1.1: The different components of the Boundary Layer [2].

The boundary layer equation can be derived using the Navier-Stokes equation[3]. Where the non dimensionalized Navier-Stokes equation can be written as [3]:

$$[St]\frac{\partial \vec{V}}{\partial t} + (\vec{V}\cdot\vec{\nabla})V = -[Eu]\vec{\nabla}P + \left[\frac{1}{Fr^2}\right]\vec{g} + \left[\frac{1}{Re}\right]\nabla^2\vec{V} \quad \text{(eq.8)}$$

Where V is the velocity, P is the pressure, and g is gravity. The equation also calls for the Euler number Eu, as well as the Froude number Fr, and Strouhal number St. By neglecting the effects of gravity as well as the unsteady term the equation is written as:

$$(\vec{V}\cdot\vec{\nabla})V = -[Eu]\vec{\nabla}P + \left[\frac{1}{Re}\right]\nabla^2\vec{V} \quad \text{(eq.9)}$$

As Cengle explains, the value of Eu = 1 due to the lack of pressure difference determined by the Bernoulli equation [2]. By non dimentionalizing the variables used in the x-component of the Navier-Stokes equation it is possible to write the equation as:

$$u\frac{\partial v}{\partial x} + v\frac{\partial u}{\partial y} = -\frac{1}{\rho}\frac{\partial P}{\partial x} + v\frac{\partial^2 u}{\partial x^2} + v\frac{\partial^2 v}{\partial y^2} \quad \text{(eq.10)}$$

$$u^*\frac{\partial u^*}{\partial x^*} + v^*\frac{\partial u^*}{\partial y^*} = -\left(\frac{L}{\delta}\right)\frac{\partial P}{\partial x} + \left(\frac{v}{UL}\right)\frac{\partial^2 u}{\partial x^2} + \left(\frac{v}{UL}\right)\frac{\partial^2}{\partial y^2} \quad \text{(eq.11)}$$

Where the values for u^*, v^*, x^*, and y^* are:

$$u^* = \frac{u}{U} \quad v^* = \frac{v}{V} \quad x^* = \frac{x}{X} \quad y^* = \frac{y}{\delta} \quad \text{(eq. 12)}$$

It is possible to determine the boundary layer height by analyzing the mass flow deficit[2]. Where, as Hibbler [3] explains, due to the viscosity the mass flow deficit can be written as:

$$dm_0 - dm = \rho(U - u)(bdy) \quad \text{(eq. 13)}$$

Where integration of the height δ is necessary to determine the total deficit [3]. Since the values for ρ, b, and U are all constant, the resulting equation can be:

$$\delta = \int_0^\infty \left(1 - \frac{u}{U}\right) dy \quad \text{(eq.14)}$$

Although, to determine the displacement thickness, it is necessary for the velocity profile of u=u(y) to be known. For this reason, the use of Blasius' solution for u/U can be utilized for the calculation of the integral. This results in equation 15 which can be used to calculate the thickness of the boundary layer for laminar flow.

$$\delta = \frac{4.91x}{\sqrt{Re}} \quad (eq. 15)$$

Furthermore, by taking advantage of Prandlt's one-seventh power law [3], the same calculation can be done for turbulent flow using equation:

$$\delta = \frac{0.16x}{(Re)^{\frac{1}{7}}} \quad (eq. 16)$$

1.5 Computational Fluid Dynamics

For this study, computational fluid dynamics (CFD) is utilized in order to achieve approximate solutions to the governing equations which allow the analysis of fluid flow. With the use of user specified boundary conditions these partial derivative equations can be solved [4]. CFD works on different methods to solve the governing equations of momentum, continuity, and energy [5].

$$\frac{\partial \rho}{\partial t} + \nabla \cdot \rho \vec{u} = 0 \qquad (eq.17)$$

$$\frac{\partial}{\partial t}(\rho u) + \nabla \cdot \left(\rho \vec{u} \vec{V}\right) = -\nabla P + \rho \vec{f} + \nabla \cdot (\bar{\tau}) \qquad \text{(eq. 18)}$$

Where the value τ is the stress tensor, which for Newtonian fluids is demonstrated by:

$$\tau_{ij} = \mu \left(\partial_j u_i + \partial_i u_j - \frac{2}{3}\delta_{ij}\partial_k u_k\right) + \delta_{ij}\lambda \partial_k u_k \qquad \text{(eq. 19)}$$

With the use of the software AcuSolve by Altair the simulation of the different vehicle models can be achieved with high accuracy. This software works on a finite element method that uses a specified fluid domain, which then gets divided into a subdomain or mesh. The turbulent model used in this system is the Spalart-Allmaras one-equation model which is demonstrated by the equation:

$$\frac{\partial \tilde{v}}{\partial t} + u_j \frac{\partial \tilde{v}}{\partial x_j} = C_{b1}[1 - f_{t2}]\tilde{S}\tilde{v} + + \frac{1}{\sigma}\{\nabla \cdot [(v + \tilde{v})\nabla v\} + C_{b2}|\nabla v|^2\} - \left[C_{w1} f_w - \frac{C_{b1}}{k^2} f_{t2}\right]\left(\frac{\tilde{v}}{d}\right)^2 + f_{t1}\Delta U^2 \quad \text{(e.q.20)}$$

This turbulent model is more effective in low Reynolds number incompressible flow applications, compared to other turbulent models such as k-ϵ turbulent model [6].

1.6 Richardson Extrapolation

When working with CFD it is important to assure the resulting values are not affected by the quality of the mesh being used. For this a mesh independence study can be conducted, where the value of the element size is reduced by half, then results are compared in order to assure the values are independent of the mesh quality [5]. However due to the nature of CFD there is always an amount of error involved with the mesh. This mesh error can be calculated using the Richardson extrapolation [7]:

$$A = A(h) + a_0\, h^{k_0} + a_1 h^{k_1} + \cdots \qquad \text{(eq. 21)}$$

Where the value of A is the exact solution, h is the element size, and a and k are constants. Since the element size is the value decreased at a certain step size. The value h tends to be divided by h/t where the value t is the desired step size usually t=2 [7]. This means the equation can be rewritten as:

$$A = A\left(\frac{h}{t}\right) + a_0\left(\frac{h}{t}\right)^{k_0} + a_1\left(\frac{h}{t}\right)^{k_1} + \cdots \quad \text{(eq.22)}$$

A mesh independence is usually conducted by decreasing the element size twice, which results in three different mesh sizes being compared [5]. These three different mesh sizes are used to solve for the mesh error using the Richardson extrapolation. This calculation was accomplished with the use of a code on the technical computing software Mathematica.

1.7 High Power Computing

High power computing (HPC) involves the use of computing clusters in unison to increase computational power. This is done by taking advantage of parallel computing environments such as Intel MPI in order to scale the workload through multiple computing nodes. For this study the use of HPC systems is utilized in order to compute large CFD simulations.

The HPC system used was the Lonestar 5 system from the Texas Advanced Computing Center (TACC) located in the University of Texas at Austin. This system utilizes 1252 Cray XC40 compute nodes, which use dual 12 core Intel Xeon E2690 v3 processors [8]. For a total of 30,048 computing cores, at 24 cores per computing node.

With the use of a Slurm workload manager, jobs are submitted using a script that specifies the amount of resources desired for a particular job. Files are initially uploaded to the server using SFTP software in order to begin the meshing process. The script used to submit the job to the queue is shown in the appendix. In order to submit commands to the server, an SSH software such as putty is required. The command:

sbatch jobscript

Is then entered to begin the submission of the job to the queue, where “jobscript” is the name of the script file being submitted. By using command:

squeue -u username

where “username” is the screen name of the user, the status of the current jobs submitted to the queue can be checked. Once processed, the files can then be checked remotely, or downloaded to a local computer. However due to the size of the files, this may not be recommended due to high download times, or high recourses required to open some of the files.

While the amount of processors influences the amount of computing time, an increase in the number of processors isn’t always desirable. As Shown by the plot bellow, the amount of compute time is not linearly related to the amount of processors.

Chapter 2: Validation

2.1 Theoretical Drag

In order to validate results from the simulations, there first must be simulations done for a geometry with a known value for drag, using the same parameters. The geometry used in this validation process is a sphere, which has known values for drag and lift. The theoretical values for the drag force as well as lift force acting on a sphere can be calculated using the following equations [2]:

$$F_d = \frac{1}{2}\rho V^2 C_d A \quad \text{(eq.23)}$$

$$F_l = \frac{1}{2}\rho V^2 C_l A \quad \text{(eq.24)}$$

In order to solve these equations, the known conditions for the current vehicle are used, which can allow to simulate similar conditions in the validation. The vehicles velocity must average 15mph due to the regulations of the Shell Eco-marathon competition[9]. This gives an inlet velocity of 15 mph which is converted to 6.7056 m/s. The density ρ is the air density which the software assumes to be $1.225\ kg/m^3$. When calculating the surface area A, the equation $A = \pi\frac{D^2}{4}$ can be used in order to get an exact value for the surface area.

This calculation also requires a value for the drag coefficient Cd which can be acquired using experimental data that documents these values. A sphere's drag coefficient can vary greatly depending on the Reynolds number. Looking at the figure below which shows the drag coefficient of a sphere in relation to the Reynolds number, it is visible how the drag coefficient of a smooth sphere can vary. Commonly the Value for a Cd of a Sphere in Laminar flow for Reynolds values less than $Re \leq 2 \times 10^5$ can be Cd = 0.5 [2], and for Reynolds values more than $Re \geq 2 \times 10^6$ normally the drag coefficient is Cd = 0.20 [2].

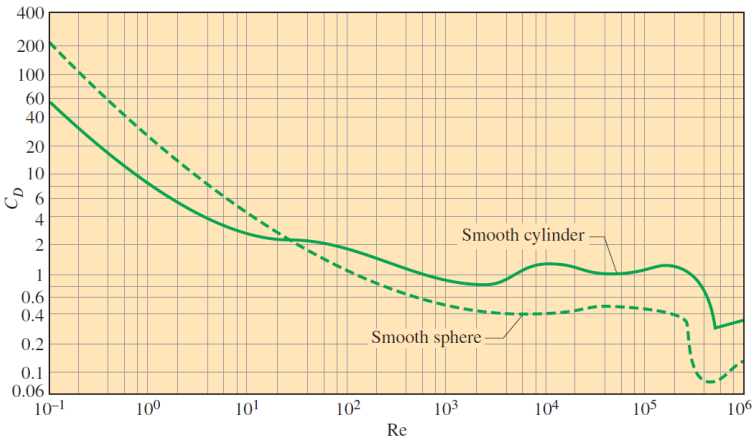

Figure 2.1: Drag coefficient of a sphere relative to the Reynolds number [2]

In order to know the values for the size and parameters of the simple geometry, the Reynolds number of the current vehicle must be calculated. This gives relatable values for turbulence in both the simple geometry and the actual vehicle. When calculating the Reynolds number for the current vehicle, the following equation is used:

$$Re = \frac{VL}{\nu} \qquad (eq.25)$$

Where V is the vehicle velocity of 15 mph which is converted to 6.706 m/s, and ν is the kinematic viscosity of air at the assumed temperature of 75°F which is $1.562x10^{-5}\ \frac{m^2}{s}$ according to the table used [2]. In this case the characteristic dimension used would be the vehicle length which is 2.286 meters as measured on the current vehicle. These parameters yield a Reynolds Number of 9.81×10^5, which shows the flow of the air is at a transient state. However, for the parameters considered, the Reynolds number $Re \approx 1 \times 10^6$ is between the values for laminar and turbulent drag coefficients. The drag of a sphere in this range tends to drop dramatically and has strange behavior. However, going by figure 2.1 the value of drag for the given Reynolds number is Cd = 0.15.

Simulation of this range proved to have many issues, therefor, the validation is conducted at a lower Reynolds number of $Re = 10^4$ where the flow is much more laminar and its behavior

is more predictable. This means the values of the velocity change to 0.63 m/s, and the drag coefficient is Cd=0.40 according to figure 2.1.

Solving for the diameter of the sphere in the Reynolds equation yields:

$$D = \frac{\nu Re}{V} \qquad (eq. 26)$$

Which gives the diameter necessary for the sphere in similar conditions. Which in this case will be equivalent to the length of the vehicle. This defines the parameters for simulating the validation. There must be a sphere of diameter 2.286 meters with a velocity inlet of the fluid of 6.706 m/s. using this new found diameter it is now possible to calculate the frontal area which is shown on the calculation:

$$A = \pi \frac{D^2}{4} = \pi \frac{(2.86\ m)^2}{4} = 4.104\ m^2 \qquad (eq. 27)$$

With these values it is possible to calculate a theoretical drag force which can then be compared to the resulting values from the simulation.

The virtual wind tunnel software automatically calculates an approximation of the frontal area. This is accomplished by projecting the geometry towards the front or inlet of the wind tunnel [5]. This area is usually an approximation and many users will input the value manually. The value calculated for this particular geometry, is A = 4.230 m2 which is a 3% difference from the actual value.

The mesh for the sphere was generated using R-Tria elements with Hypermesh. The element size was set automatically to .09m generating an element count of 4446. This was a starting point from where the refinement of the mesh for the geometry will be refined from.

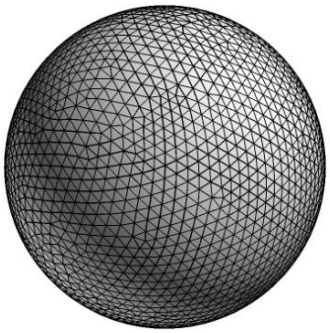

Figure 2.2: Mesh of Sphere

2.2 Fluid Domain

The simulation was first ran using the 2.286m sphere, and the initial boundaries of the wind tunnel where then adjust it to fit the sphere comfortably. The boundaries were initially set to 8m width, 8m height, and 45m length. The far field mesh was set to a size of 0.20m the boundary layer height was set to .00252m, which generated a mesh of about 3.1 million elements. This resulted in a drag coefficient, of 0.141 and a lift coefficient of -0.082. In order to minimize the effects due to the distance of the boundaries, the ratio between the fluid domain width vs the sphere diameter is increased. The same simulation was then ran with the same condition, however the boundaries were increased by 2m. Having a boundary of 10m width, 10m height, and 45m length, resulting in a width/diameter ratio of 3.94. This process is repeated while doubling the increase in size, until an optimal ratio of width vs diameter is found.

The following plot demonstrates the changes of the resulting drag coefficient as the fluid domain is increased in size. The value of drag decreases significantly as the boundaries of the fluid domain are increased initially, then begin to show a diminished decrease as the domain continues to increase.

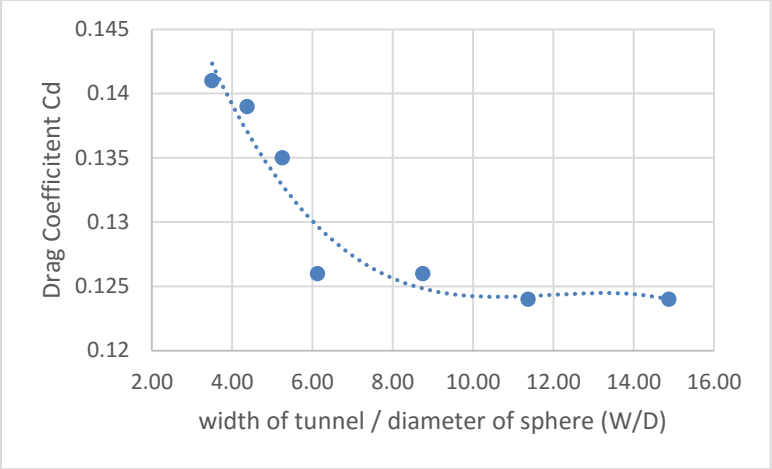

Figure 2.3: Plot of Resulting Drag Coefficient against ratio W/D.

The results show an optimal value for W/D is any value greater than W/D=10 in order to minimize effects due to the fluid domain. This increase in size will in turn also drastically increase the number of elements being generated, thus increasing solving time.

2.3 Boundary Layer

The software allows different parameters for the boundary layer to be simulated with higher accuracy. A global boundary layer can be used throughout the geometry, as well as the ability to specify different boundary layer parameters for different areas in a complex geometry. In order to set the proper parameters for the global boundary layer parameters to be used, the boundary layer height for the geometry needs to be estimated. Using the equations:

$$\frac{\delta}{x} = \frac{4.91}{\sqrt{Re}} \qquad (eq.28)$$

$$\frac{\delta}{x} = \frac{0.16}{(Re)^{\frac{1}{7}}} \qquad (eq.29)$$

The boundary layer thickness can be calculated for a laminar flow (eq. 28), as well as turbulent flow (eq.29) [2]. Since the flow being used is just above transitional, the equation for turbulent flow can be solved to have an estimate boundary layer height. This yields a boundary layer height of δ= .0255 m. Having this information allows for a proper adjustment of the

boundary layer parameters. The two main parameters which inform the solver of the boundary layer are “First Layer Height” as well as “Layers”. The First layer height is automatically calculated by the software as .00252m, and automatically set to 5 layers which make for a good starting point.

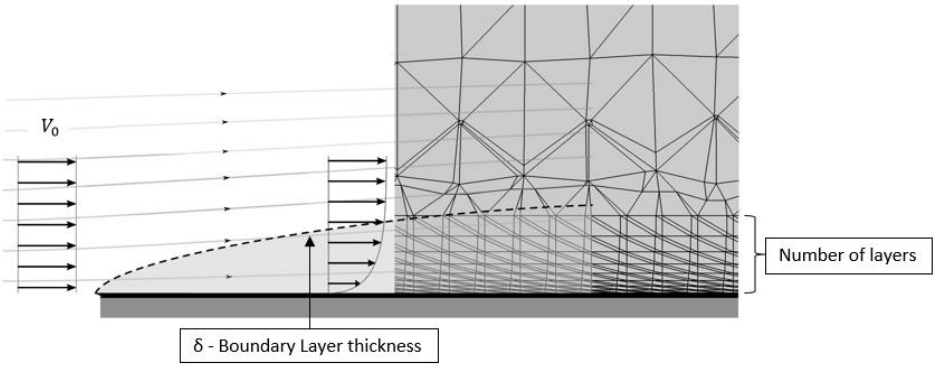

Figure 2.4: Boundary layer refinement

The number of layers defines a number of elements within the Boundary layer. This number was initially set to 1 then increased slowly in order to achieve an accurate boundary layer refinement. Using a ratio between the boundary layer height and the first boundary layer height, it is possible to find an appropriate number of elements to have within the boundary.

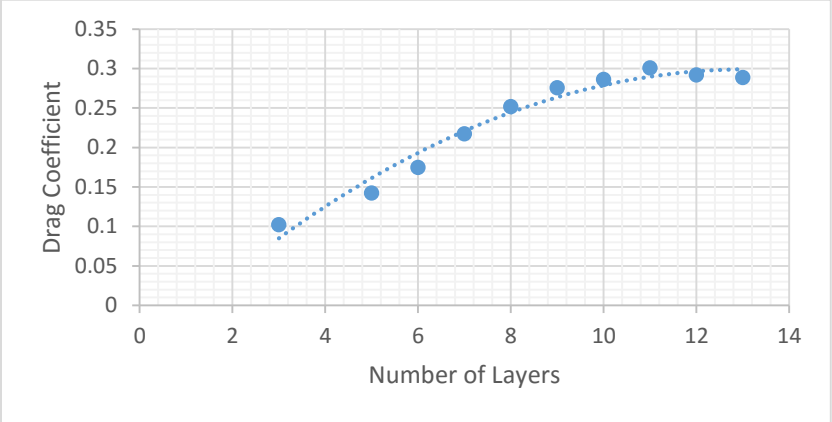

Figure 2.5: Drag coefficient against number of layers

Plotting out the resulting drag coefficients vs the amount of layers used, it is visible how the values begin to converge at a specific point. Showing that a further increase in the number in layers does not improve results beyond a certain point. However, this can greatly affect the computational work load with an element increase of about 5-10% for each layer. From these results it is clear that an optimum value of elements should be used that is greater than 10 in order to assure proper refinement with in the boundary layer.

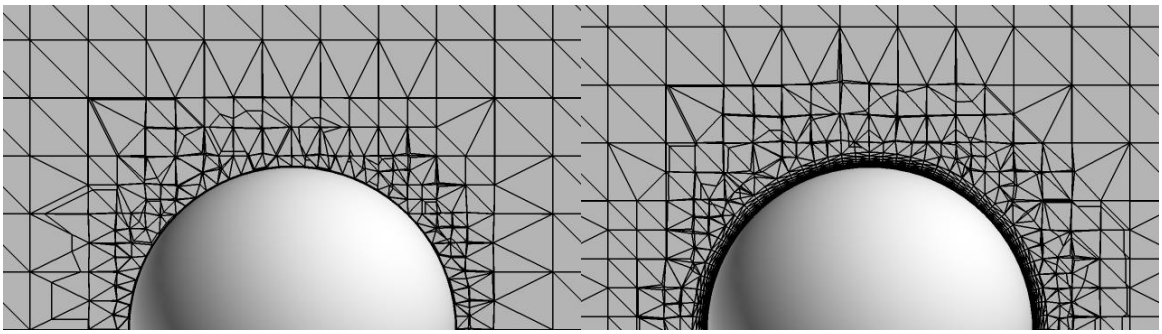

Figure 2.6: Comparison of 2 layers and 10 layers

The value used for number of layers can also be used to assist with convergence. From experimental results, change the value by 1 or 2 layers in many cases allowed for improved convergence of the simulation results. Using these results it is possible to calculate an adequate value for these parameters using the equation:

$$L_1 \cdot GR^L = \delta \qquad \text{(eq.30)}$$

Where the first layer height L_1 is multiplied by the growth rate GR which is set by the software to a value of 1.3. It is then possible to find the number of layers L by using the calculated boundary layer height δ.

2.4 Mesh Refinement

In order to eliminate any error caused by the global mesh size, it is important to perform a mesh independence study [5]. Where refining of the mesh by decreasing the element size by half, allows to assure the results are not affected by the quality of the global mesh. Typically, at least

three different mesh sizes are used in order to assure a proper resolution [5]. The results from these values are then used in the Richardson extrapolation, in order to calculate the error caused by the mesh refinement.

The element size for the original mesh is set to a value of 0.40m and then decreased to 0.20m and finally decreased to 0.10m. This will allow the mesh independence study to be conducted in order to minimize the error due to the global mesh. The resultant values for these simulations are then utilized in order to calculate the resulting drag force.

Diameter	Front Area	Velocit	Density	Layers	Far Field	Drag Co	Drag Force	%Error
2.286	4.23	0.63	1.225	12	0.4	0.465	0.478	16%
2.286	4.23	0.63	1.225	12	0.2	0.421	0.433	5%
2.286	4.23	0.63	1.225	12	0.1	0.41	0.422	3%

Table 2.1: resulting values for the mesh independence study

The calculated drag force is then used to find the error between the theoretical value and the simulated results. As visible by table 2.1, the value for the error decreases as the element size is decreased. However, the change in error decreases as the element size is decreased. This means the value for the exact solution would be achieved at an infinitely small size element. In order to account for this error, the Richardson extrapolation is used.

The Richardson extrapolation is calculated using a Mathematica script, as shown in the appendix. This code then generates a plot which shows the convergence of the values as the element size reaches 0.

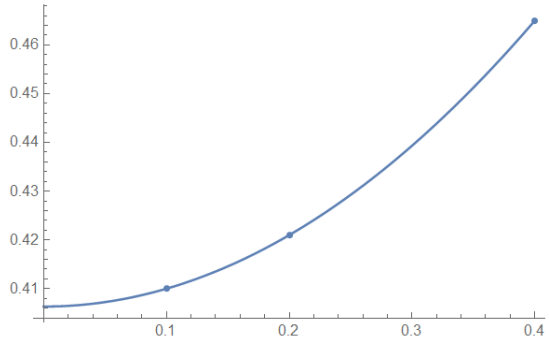

Figure 2.7: results for the Richardson extrapolation from a Mathematica code

According to the calculation, the resulting drag force $F_{sphere} = 0.422 \pm 0.36\%$. The resulting error for these parameters is 3% as shown by table 2.1.

2.5 Ideal Simulation Parameters

From this study the ideal parameters are noted in order to assure accurate simulation of the vehicles body. In order to reduce effects of the fluid domain, the ratio between the body's width and the domain boundaries must be maintained at a ratio of $\frac{W}{D} = 10$. Using the equation 30 the ideal number of layers can be calculated.

Chapter 3: Wheels In vs Wheels Out

3.1 Introduction and Background

When considering a design with wheels in vs wheels out, many advantages and disadvantages need to be considered. While the design with wheels out may have a lower frontal surface area, there is an increase of drag due to the geometry of the wheels. The total drag of a moving body is increased drastically when wheels are added. According to W. Hucho, the wheels on a vehicle can amount to half of the vehicles total drag [13]. This can be a substantial source of drag in a vehicle designed for maximum fuel efficiency, which might have a streamlined body with a relatively low drag coefficient.

Many characteristics of a wheel can cause large increases in drag. Due to the fact that wheels tend to lack a streamline geometry, the flow around the wheel tends to behave in a very strange manner. A wheel begins to show its lack of aerodynamic characteristics when considered as a thin cylinder [13]. Cylindrical geometries tend to have a lack of streamlined flow, which is evident with the large amounts of wake behind the geometry [13]. The wake is mostly due to the low pressure area created as a result of the separation of the flow, which results in a large amount of form drag [2]. Due to the finite width of the cylinder there are two vortices that form, as mentioned by W. Hucho [13]. These vortices tend to develop toward the top and the bottom of the wheel hanging over the edges of the wheel. One thing to be noted, as Hucho mentions, the direction of the vortices can change [13]. This is due to the edges of a cylinder in contrary to the round edges of an actual vehicle wheel [13].

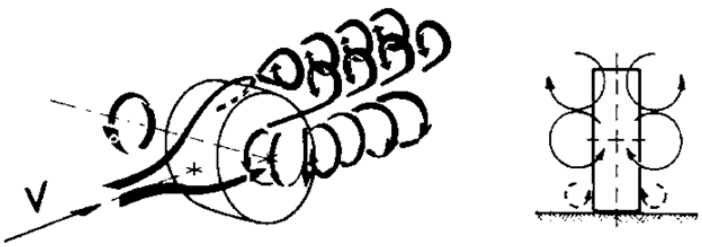

Illustration 3.1: Vortices created around an open wheel [10].

A wheel's rotation will also cause drops in the drag coefficient. This is due to a difference in the pressure within the wake region, between a stationary wheel and a rotating one [10]. While a wheel sits on a surface, the rotation causes air to be pushed out from the stagnation point between the ground and the bottom front of the wheel. This fluid being forced out increases the magnitude of the bottom vortices, which allows for improved flow towards the wake region [13]. One way to reduce the drag of a wheel its self, is by utilizing wheel covers that reduce the negative effects of the fluid through the spokes of a wheel. The resulting drag from a covered wheel is minimal for a stationary wheel, however the value of drag for a rotating covered wheel is a more substantial decrease [10].

While the effects of fluid flow over an open wheel seems to make a more favorable argument towards the use of wheels covered by the vehicle's fairing, there are other negative effects involving wheels in, which may be more significant than those caused by open wheels. The most evident difference is the large increase of frontal surface area. While it is possible to maintain a streamline design with a low drag coefficient, the technicalities of allowing enough room for the wheels within the body cause a large increase in frontal projected area leading in an increase in the drag force acting on the vehicle.

There are different effects involving the use of wheels integrated in a body which are less intuitive. One effect involves the flow around a wheel inside of a wheel well. This effect tends to be minimal depending on the volume of air inside the wheel well vs the volume of the wheel, as studied by A. Cogotti [10]. These results show that the lower the ratio of volumes between the wheel well and the wheel, the lower the effects of drag as show in the plots from the study [10].

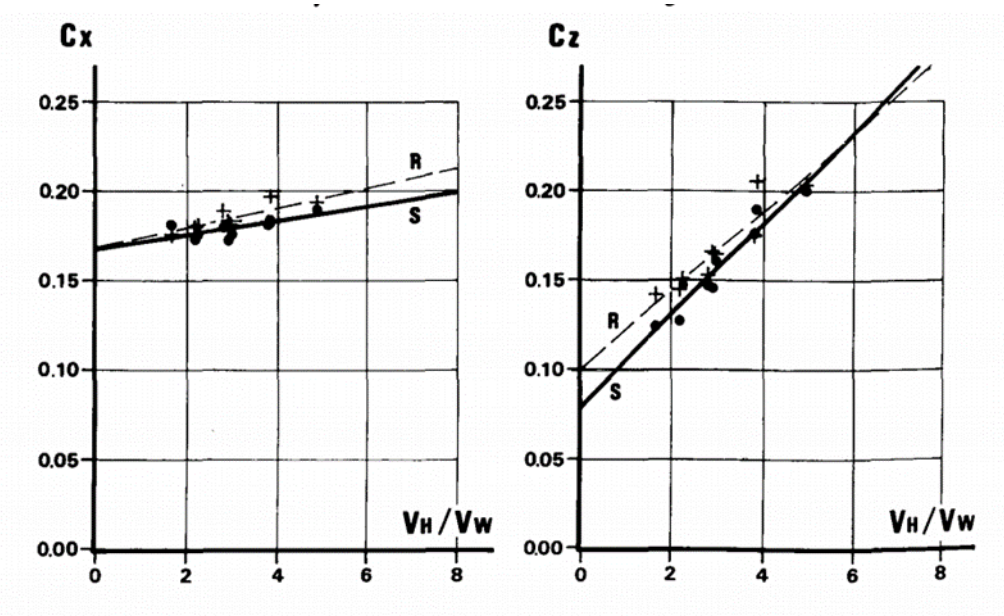

Figure 3.1: Example of Heading [10].

While the effects of the wheel well can be considered minimal, there is one other effect which can cause large amounts of drag. As W.Hucho mentions, while the flow of the air over the body is well understood, there is much less known regarding the underbody of a vehicle [12]. He continues to mention how the flow of the fluid moving down the underbody of a passenger vehicle moves from the middle of the body, outward towards the sides of the vehicle [12]. These effects of the flow will cause the moving air to hit the vehicle wheels at a yaw angle rather than head on, leading to large increases of drag. These effects are dependent on the amount of overhang of the vehicles front end from the wheels [12]. While this may be a concern for both a vehicle with wheels in and one with wheels out, this effect is more predominant on a vehicle with wheels in. This can be due to the negative pressure that forms within the wheel well [12]. Studies done on these effects, such as the one by J. Wiedemann show the increase of the drag coefficient for a wheel to be more than double than that of a wheel with a yaw angle of 0 [17].

The effects of drag caused by wheels can be very complex, and requires a large amount of study. Even though the behavior of flow over a wheel is beyond the focus of this study, this

can be a good topic for another study. However, due to these effects it is important to compare the resulting drag forces of both wheels in and wheels out.

3.1 Wheels Out

In order to find a general idea in what the main differences in drag force would be when comparing wheels out or wheels in, basic drag force calculations can be done. This process is begun by choosing a general geometry that would be adequate for this type of application. It is advantageous to choose a geometry which is well documented. Two main types of geometries which can be considered are Ellipsoidal and streamline geometries. This is due to the relatively low coefficients of drag involved with them. When deciding between these two geometries, an ellipsoid can be more favorable due to the ease of adaptation to the existing vehicle, and more comparable geometry. In order to have calculated values which can be related to this application, the general dimensions are based on the current vehicle.

In calculating the drag force acting on a vehicle with wheels out, there must be a calculation of the drag force acting on body of the vehicle as well as one for the force acting on the wheels. This process is begun by calculating the Reynolds number of the flow over the body. The length of the existing vehicle is 8ft or 96 in. This is the characteristic length to be used in the calculation of the Reynolds number. Calculating this value will show if the flow is turbulent or laminar.

Reynolds number for the body can be solved with the equation [2]:

$$Re = \frac{VD}{\nu} \qquad (eq.31)$$

Where the kinematic viscosity is $\nu = 1.56 * 10^{-5}$ and the velocity is V= 15mph or 6.706 m/s . This yields a Reynolds number of $Re = 10^{6}$.

When working with a geometry such as an ellipsoid or streamline body, the drag coefficient can vary greatly depending on the ratio between the length L and the diameter D of

the shape. This ratio is known as the fineness ratio, where: fineness ratio=L/D. While a thin long ellipsoid may seem favorable, there is a range in which the difference in length and diameter can be too small or too large. Since the total drag coefficient Cd is the combination of the form drag and the skin drag, the value Cd can be equated to $C_d = C_{form} + C_{skin}$. When the value for L/D is too small, the form drag of the geometry dominates the total value for drag. However, having an extremely slim and long ellipsoid or streamline body can become an issue as well. When the value for L/D becomes too large, there is a substantial increase in the amount of skin drag which will also lead to a high value for the drag coefficient Cd.

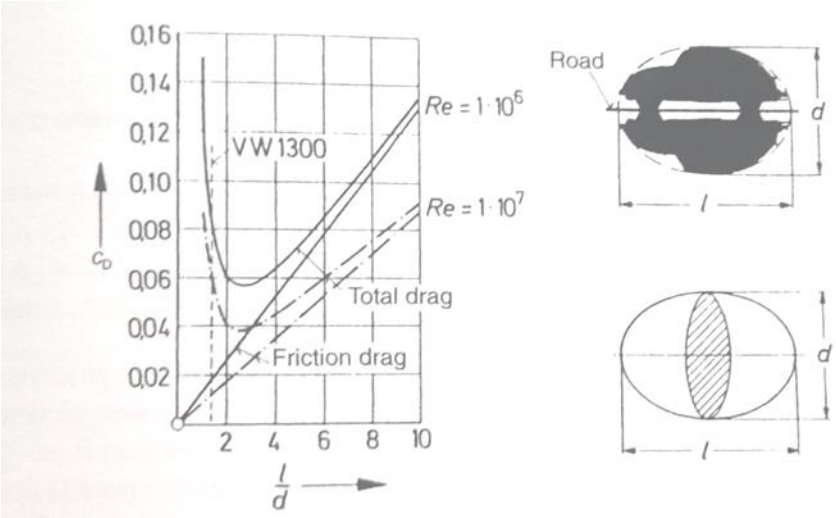

Figure 3.2: Plot of the Drag Coefficient of an Ellipsoid [13].

While working with an ellipsoid the optimum fineness ratio appears to be L/D= 2.5, when looking at figure 3.2. Having a vehicle length of 96in, this would result in a diameter of 38.4 in. However, a diameter of 38.4in would be much too wide to accommodate the vehicles height requirements as well as affect the ground clearance of the vehicle. Therefor a slight increase in the fineness ratio must be used, at the cost of a slight increase in the drag coefficient. The best compromise between these two factors appears to be in the range of L/D = 4. At this point the vehicles current dimensions will have a much more compact fit.

Solving for diameter of the body when wheels are out using the desired fineness ratio, is done as follows: D= 96in/4, and gives a minor diameter of D= 24in (.609m) where the value for the drag coefficient is Cd= .065. Having the value for Cd it is possible to calculate the drag force acting on the vehicles body. The Drag force of the Body is calculated using the equation:

$$F = \frac{1}{2}\,\rho V^2 C_d A \qquad \text{(eq.32)}$$

Where the density is ρ=1.225 kg/m^3 And the velocity is V= 15mph or 6.706 m/s. Based on the geometry of the new found dimensions the projected frontal area for the body with wheels out is calculated with: $A_{wo} = \pi R^2$ which yields:

$$A_{wo} = \pi(.304m)^2 = .290m^2 \qquad \text{(eq.33)}$$

Plugging in all the given values to the drag force equation gives the force of the body:

$$F_B = \frac{1}{2}\left(1.225\frac{kg}{m^3}\right) * \left(6.706\frac{m}{s}\right)^2 * (.065) * (.290\ m^2) = .487N \qquad \text{(eq.34)}$$

Once the drag force is found, the drag of the wheels is calculated individually then added for a total drag force of the vehicle. While the value of drag force for the body is small, the largest contribution of drag is from the wheels which is calculated next..

3.1.1 Drag of Wheels

In order to simplify the calculation of the drag force of the wheels, it is assumed that the wheel is a thin cylinder. This allows the usage of plots and documentation for drag coefficient of a smooth cylinder. One of the best tires used currently in the competition, is the Michelin 44-406 Prototype tire. This is the type of wheel used currently on the vehicle as well as in most of the top competing vehicles. Due to this, the calculations and all simulations will be based on the use of the dimensions of these tires.

The Michelin 44-406 Prototype tires, are a special non production tire that was design for its use in a super millage vehicle. This specific tire has a rolling resistance of 2kg/tonne, and

measures 20 inches in diameter by 1.75 inches in width. In order to find the drag force acting on each wheel, a similar approach is taken. For the wheel the characteristic length would be the diameter, therefor the Reynolds equation is as follows:

$$Re = \frac{VD}{\nu} \qquad (eq.36)$$

Where the wheel diameter is D= 20in (.508 m) and the Wheel thickness is W= 2in (.0508m) at its widest point. Since the fluid continues to be air at the same temperature, the kinematic viscosity is $1.56 * 10^{-5} \frac{s}{m^2}$. There for calculating the Reynolds number for the wheel would be:

$$Re = \frac{\left(6.706 \frac{m}{s}\right) * (.508\, m)}{1.56 * 10^{-5} \frac{s}{m^2}} = 218{,}375 \qquad (eq.37)$$

Using the calculated Reynolds number, it is possible to find the drag coefficient for the cylinder using the following plot.

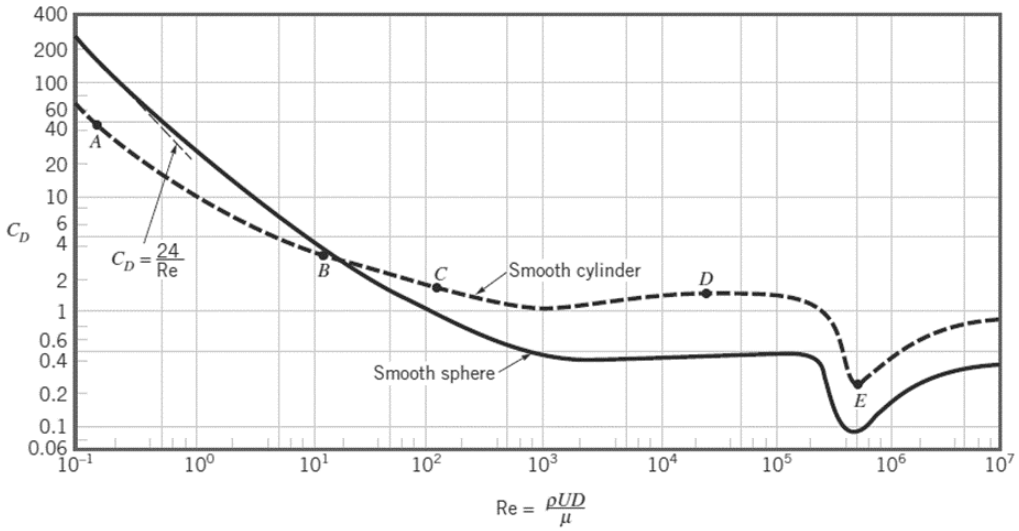

Figure 3.3: Values of Drag coefficient for a relative Reynolds Number for a sphere [3].

Based on the Reynolds number $Re = 2.18 \times 10^4$ the drag coefficient of the cylinder is close to Cd=1.0. using the equation for drag force, it is possible to find the drag force of each wheel. Where the Frontal Area of wheels is $A = D \times W = .0258\, m^2$. The velocity V and the

density ρ are the same values used in the calculation of the body. Therefor the drag force of a wheel would be:

$$F_w = \frac{1}{2}\left(1.225\,\frac{kg}{m^3}\right) * \left(6.706\,\frac{m}{s}\right)^2 * (1.0) * (.0258\,m^2) = .711\,N \quad \text{(eq.38)}$$

3.1.2 Total Drag

With the drag of the body and the drag of each wheel, the total drag can be found by simply adding the drag forces of all the components together. This includes the body as well as the 3 different wheels.

$$F_{total} = F_B + 3F_w \quad \text{(eq.39)}$$

$$F_{total} = (.487\,N) + 3 * (.711\,N) = \mathbf{2.62N} \quad \text{(eq.40)}$$

This calculation gives a general idea of the resulting drag force for the case specified; the actual values may vary due to several factors that were not accounted for in the calculation. These include effects of the wheels rotating which can account for an increase of about 10 % like those seen in the study done by A. Cogotti [10]. There are other effects such as those of the ground affecting the flow near the body due to the vehicle height, which is ignored in the calculation for simplicity. However the study of the ground effects is discussed further in a different section.

3.2 Wheels In

When considering the main differences in design of a vehicle with wheels in, where the wheels are covered by the external shell of the body, and an open wheel vehicle with wheels out, there are several factors to account for. The main difference which may account for the largest increase in drag is the increase in projected frontal area. In order to cover the wheels with the body the geometry needs to be stretched to the sides. This has many effects on the geometry which also affect the drag. The ideal case would be to cover the wheels by simply making the ellipsoidal geometry wider without increasing the height. This allows for the drag coefficient to be kept about the same which simplifies the calculation for a vehicle with wheels in.

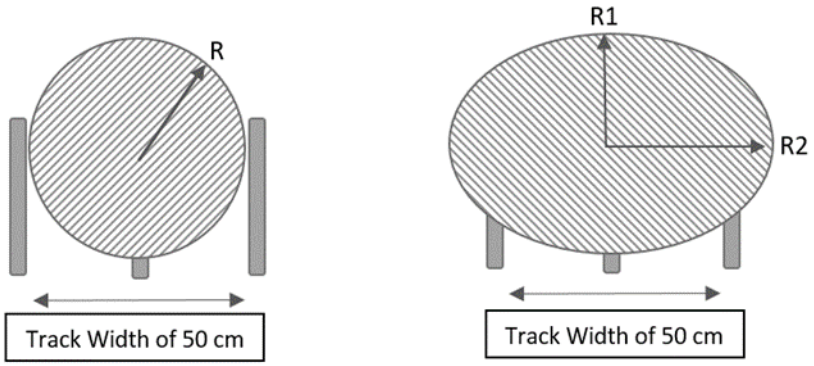

Illustration 3.2: Difference of cross sectional area for wheels in and wheels out.

The cross sectional area is elliptical, which means the projected frontal area is as well. This means the area can be calculated using:

$$A_{wi} = \pi R_1 * R_2 \quad \text{(eq.41)}$$

Where Radius 1 is the vertical radius which is $R_1 = 12\ in\ or\ .304\ m$, and Radius 2 is the horizontal radius which is R_2=19.2 in or .50 m. The value of R_2 is due to the competition regulations which state that the vehicle track width must be 50 cm [9]. Therefor the Frontal area for wheels in is

$$A_{wi} = \pi(.304m * .50m) = .478\ m^2 \quad \text{(eq.42)}$$

While finding a drag coefficient for a geometry such as this one can prove challenging, there are different assumptions that can be made in order to find a relatable coefficient. Most often these values are acquired through testing, or use of different simulation software. In order to simplify the calculation, the assumption is made, that the general geometry remains the same while only having an increase in surface area. This allows for the use of the same drag coefficient since the fineness ratio is kept close to the original value.

The drag force for the wheels in vehicle design can then be calculated using similar parameters with only a change in the Area as follows:

$$F_{wi} = \frac{1}{2}\left(1.225\frac{kg}{m^3}\right) * \left(6.706\frac{m}{s}\right)^2 * (.061) * (.478\ m^2) = \mathbf{.802N} \quad \text{(eq.43)}$$

In the case of a vehicle with wheels in the drag force is expected to be higher due to the effects of the rotating wheels in the wheel wells. These effects as well as the effects of the ground near the body are neglected for simplicity of the calculation.

3.3 Simulation of Wheels Out and Wheels In

The simulation process is begun by using the defined parameters of the calculation for the vehicle model. The vehicle model used a basic design with only the necessary detail in order to avoid any unnecessary complications further in the simulation process. The wheels used in the model are simplified as well but are designed very closely to the general dimensions of the physical wheels utilized in the vehicle. Using relatable conditions as well as dimensions, it can be possible to validate results using the calculations in the previous section.

3.3.1 Vehicle Model

The model was generated using the NX software, by making a simple ellipse of length 96 in and a height of 24 in and revolving the geometry around the center. A shaft was needed in order to have a basic mounting point for the wheels near the front of the vehicle. The position of the wheels was arbitrarily selected near the front of the vehicle. However, its position can be relatable to the current vehicles front axle positioning.

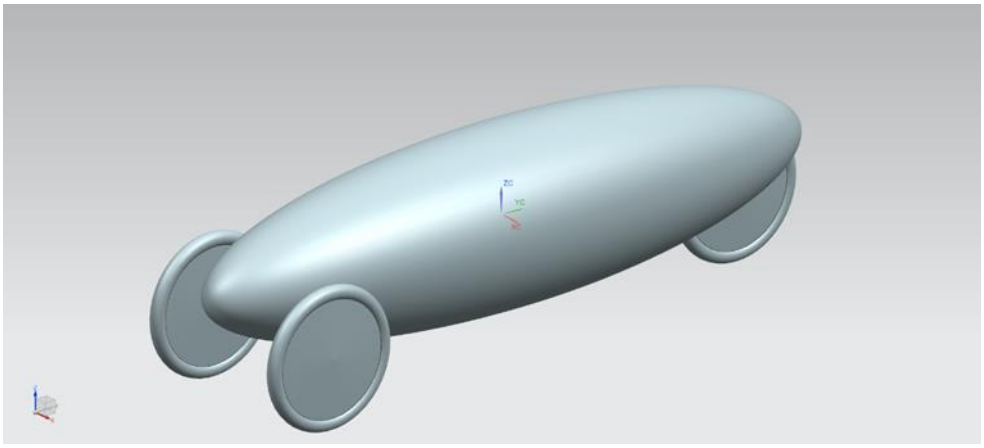

Figure 3.4: Vehicle Model of open wheel vehicle.

Due to the fact this vehicle only uses 3 wheels, which include the 2 front and 1 rear wheel, the third wheel must sit toward the center axis near the rear end of the vehicle. One very important feature that was incorporated in the model of the body is a wheel well near the rear of the vehicle for the rear wheel to sit in. This is used to avoid complications with an over lapping mesh since the rear wheel sits half way inside in the rear of the vehicle. This rear wheel well is generated as close to the wheel as possible, to minimize the effects of the fluid flow inside which can be negative.

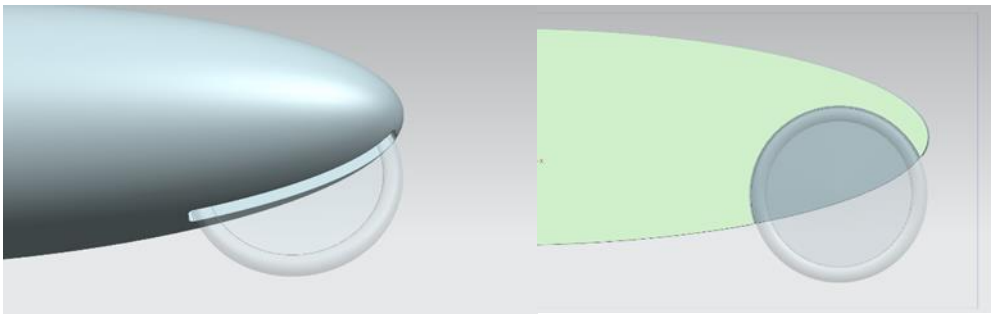

Figure 3.5: Cross Sectional view of rear wheel well.

The wheels generated are designed based on the current vehicles wheel and tire combination. The measurements taken include a 20in diameter, a 2 in width near the center with a decrease of width to 1.5 near the wheel rim, and a 1.75in width near the center of the tire. The design of the well utilizes a covered fairing design, due to the improved performance of the aerodynamics when rotating. While the rear wheel has no real mounting points, the two front wheels have simple mounting points integrated which mount to the front axle.

When modeling a vehicle with wheels in, multiple geometries were added in order to integrate the wheels properly into the vehicle. The fairing around the wheels is generated using different geometries that do not alter the positioning of the wheels, and allow for streamlining around them. While the streamline features are not entirely optimized, the basic changes should be appropriate for the focus of the study.

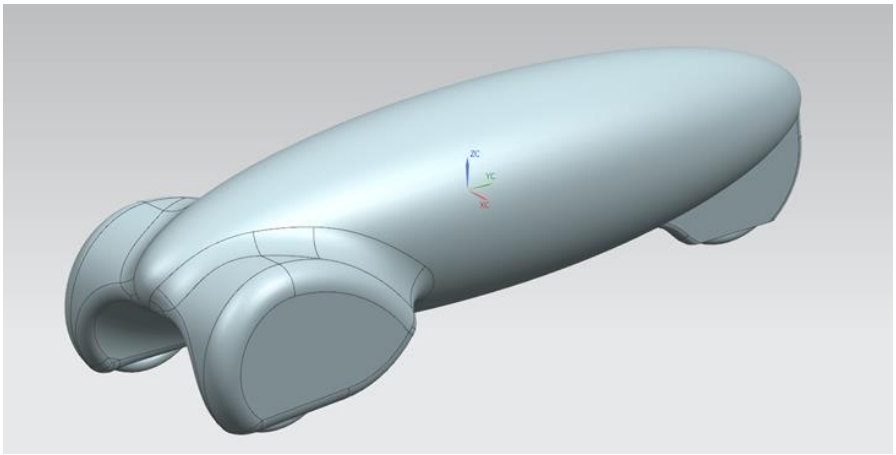

Figure 3.6: Vehicle model for integrated wheels within fairing.

Like in the previous model, the Wheel wells are kept as small as possible, in order to avoid any effects due to the flow of air within. The gap between the wheel and the wheel arches is kept close to 0.25 inch for all wheels.

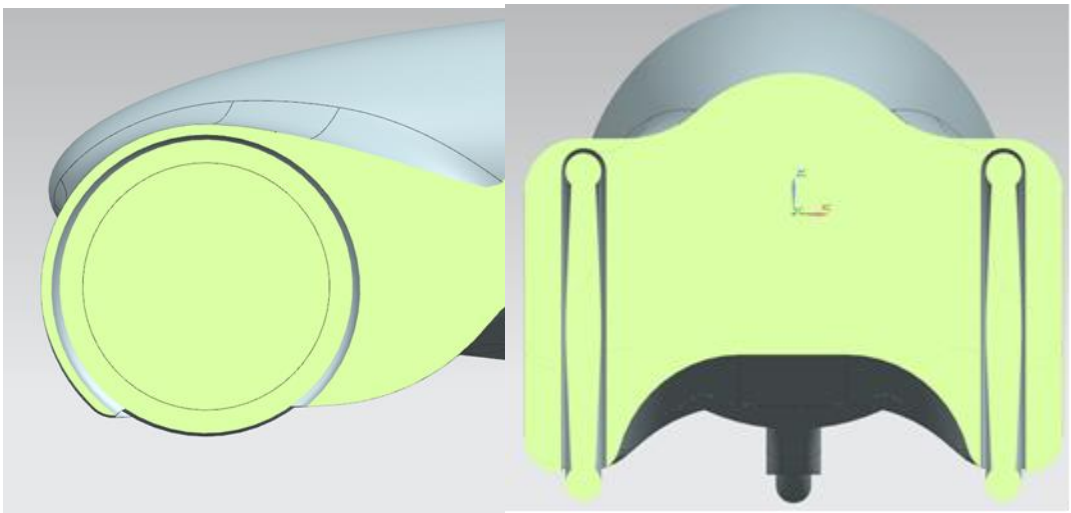

Figure 3.7: Cross Sections of front and side views for front wheel wells.

In order to maintain simplicity as well as reduce any conflicts with the simulation, the wheels are positioned with no axle attached to the wheels. However, regardless of the wheels being suspended in midair, the position of the wheel is in the exact location as the previous model.

3.3.2 Meshing of Vehicle

The meshing for this geometry is done by importing the model into Hypermesh. This is done by exporting the full assembly to and IGES file, and then opened using the Hypermesh software. Once imported, the mesh the geometry is divided into different meshes for each component. This allows for the Virtual Wind Tunnel software to be able to detect specific components of the vehicle such as the wheels, which can then be simulated rotating.

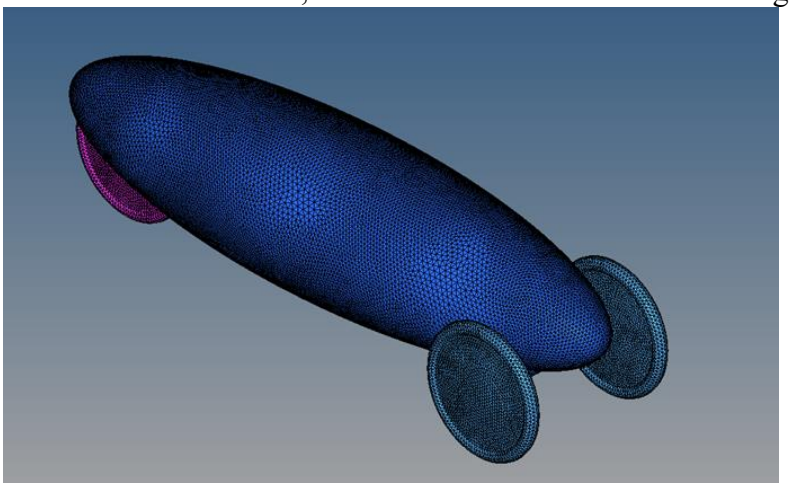

Figure 3.8: Mesh of wheels out vehicle

The mesh for the body is then modified to meet the refinements needed. This is done using a two dimensional surface mesh that is then refined and modified in order to avoid complications with the CFD software. For this mesh, is generated using first order triangular elements. The element size is set to 0.006m for a resulting element count of 62,000 elements. One important modification made, is that of the end of the front axle. With concerns of the software attempting to simulate fluid between the contact surfaces of the axle ends and the wheel center points, the two surfaces are deleted.

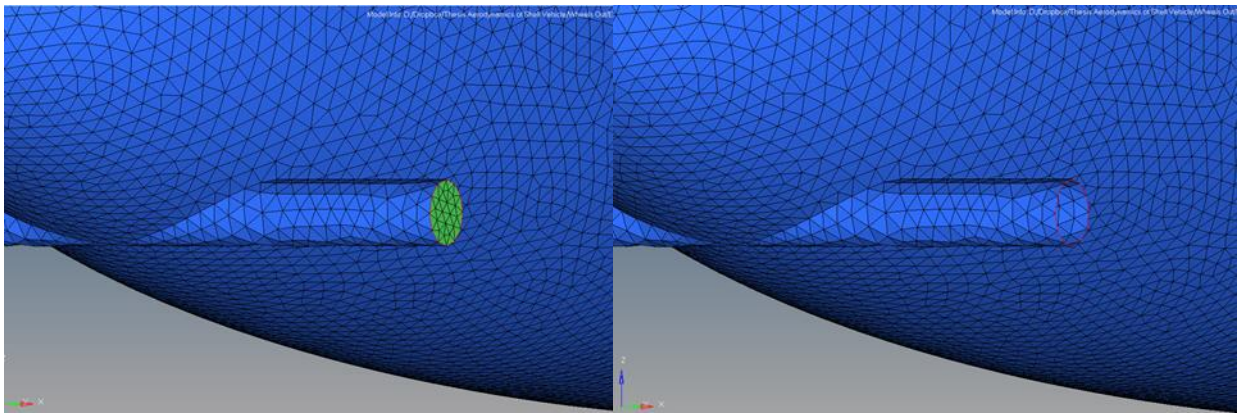

Figure 3.9: Close up of front wheel axel meshing.

While meshing for fluid simulations, there must be special attention to the interfaces of the different components that meet. In order to avoid simulation of fluids in areas intended to be sealed off. This is achieved by relating any edges in the different geometries, using equivalence options within the software to have adequate interfaces between meshes. This assures the geometry to be as air tight as possible for the fluid simulation.

Meshing the vehicle with wheels in showed less problematic since there are less interfaces between the different components of the vehicle. However, with the added features to the body's geometry, there is a larger conflict with overlapping meshes involving duplicate elements. These elements are checked and deleted using Hypermesh. The mesh for wheels in also requires a higher density element count. This is due to the increase complexity of the model, where there are more sweeps as well as rounded edges that are important for the simulation.

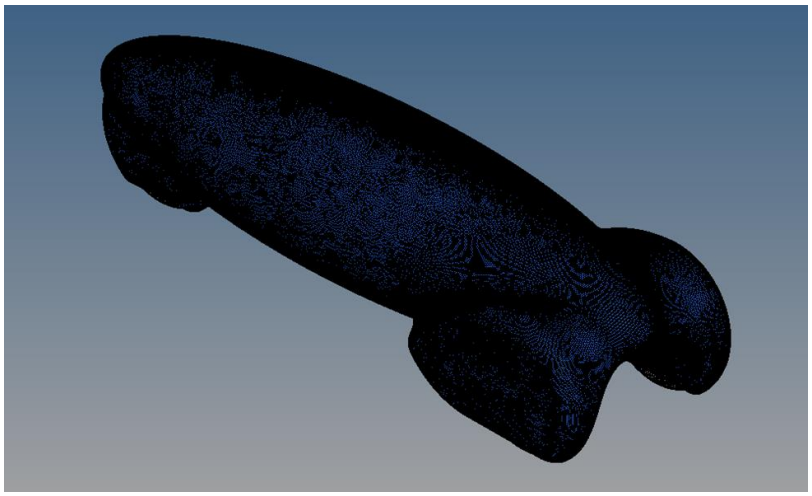

Figure 3.10: Vehicle mesh for wheels in vehicle.

The Mesh is generated using a minimum element size of .001m for a resulting element count of 405,000 elements. The mesh is also generated using first order triangular elements

3.4 Fluid Simulation

The generated geometry mesh needs to be imported to the fluid simulation software, this is done by exporting the Meshed file a Nastran Fluent solver type. With an imported file the simulation software can begin the preprocessing, solving, as well as post processing of the fluid simulation. All of the parameters selected are those found to be the most adequate during the validation process.

3.4.1 Pre-Processing

The problem set up is done with the Virtual Wind Tunnel Software. The Simulation is prepared in two different ways, one involving stationary wheels and another involving rotating wheels. In both cases the ground is simulated moving at the same velocity as the fluid inlet, where the velocity of the incoming air is set to 15mph or 6.706 m/s. The boundaries of the wind tunnel are set in compliance to the validation, where the vehicle is set 10m away from the inlet, the width is 8m, height is 5m, and the length is set to 40m.

The meshing of the fluid is adjusted globally, and is set to an initial element size value of 0.4m. This value is then refined by reducing the element size by half each time. This is done until mesh independence is clear. There are other refinement parameters used near the boundary layer, which need to be adjusted as well. The first layer height is calculated automatically by the program, and the number of layers is adjusted to this value. For the simulation of the vehicle with wheels out, the first layer value is calculated at .00254m.

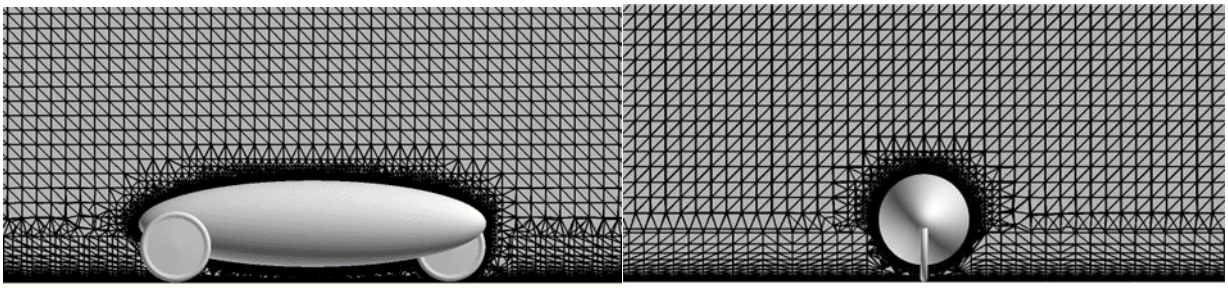

Figure 3.11: Mesh Generated for wheels out model.

The mesh is then generated resulting in a 1.9 million element mesh. This value is increased as the element size is decreased.

Similarly, the parameters when looking at wheels in are based on the validation work done in the previous section. In order to maintain consistency within the simulations, the same meshing parameters are used as in those with wheels out. The values for the global mesh are refined in the same way, although the number of elements varies from the vehicle with wheels out. When setting the value of 0.4m for the global mesh element size, the resulting element count is 6.4 million. This is due to the extra refinement the mesh for the body of the wheels in vehicle.

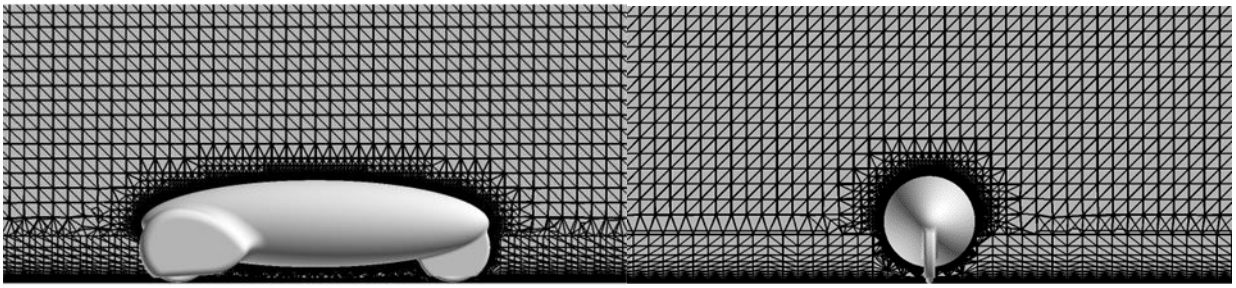

Figure 3.12: Mesh generated for wheels in model.

The refinement near the ground is not changed, due to the effects of the ground being observed in a different section. When looking at the calculated value for the projected frontal area for a vehicle with wheels in, it is equal $A_{wi} = .478\, m^2$ with the assumptions made. The value calculated by the software is equal to $A_{wi} = 0.441\, m^2$, which is an 8% difference to the calculated value. Therefore, even though the geometry is different to the original assumptions, the projected area is relatively close.

3.5 Solving

With the use of Acusolve the simulation is solved, using a high power computing (HPC) cluster. Using the Linux command:

acuRun -pb vwtAnalysis -dir ACUSIM.DIR -inp vwtAnalysis.inp -np 48 -nt 12 -do all -lsf

Will run the solver using 48 processing cores, at 12 threads per processor. Acusolve is set up to solve the Navier-Stokes equation, while using the Spalart-Allmaras the turbulence model. The convergence tolerance normally used by the solver is set to 0.001.

3.6 Results

The results are analyzed based on the resulting drag coefficient as well as resulting drag force. AcuFieldView is used in order to perform all post processing needed from the simulation results. While the software focuses on calculating the drag coefficient, this value can then be

used to calculate the drag force acting on the vehicle. With these values, the results for the drag force of both stationary wheels and rotating wheels can be compared.

3.6.1 Results of Wheels Out

As expected the values for a vehicle with rotating wheels results in a lower drag coefficient than that of one with stationary wheels. With the resulting values of each simulation plotted against the element size it is possible to see the convergence of the simulation with the increased refinement.

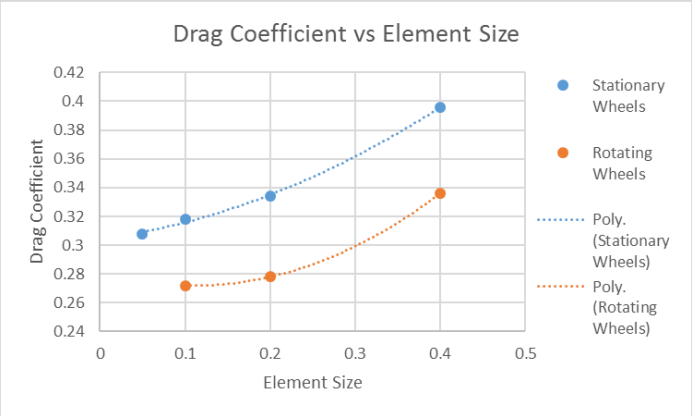

Figure 3.13: Plot of Drag coefficient vs Element size for wheels out.

The Resulting Drag coefficient for stationary wheels is Cd= 0.396, with an element size of 0.4 m and an element count of 1.9 million elements. This value converges as the element size is further decreased. The value for Cd at an element size of 0.2 m and an element count of 3.7 million elements, results in Cd= 0.334. This value begins to converge as the mesh size is further decreased by half. With an element size of 0.1m the resulting drag coefficient is Cd= 0.318. Further refinement from this point results in minimal decreases in the drag coefficient, however there is a substantial increase in the element count. As shown by the final refinement of the global mesh to an element size of 0.05m, where the drag coefficient drops to a value of Cd= 0.308 which is a decrease of 3%. However, the element count increases from 13.6 million at 0.1m, to 83.3 million elements at 0.05m, which is an increase of over 600%

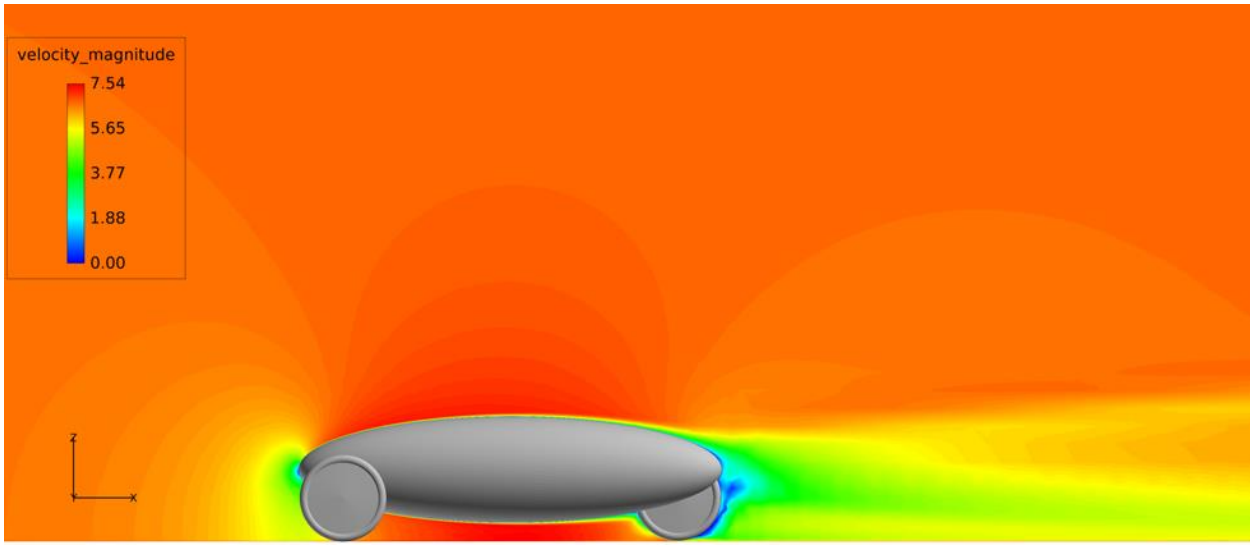

Figure 3.14: Velocity Magnitude Contour of wheels out model

The Contours for the magnitude of the velocity show the behavior of the flow around the vehicle. While the flow around the body appears to be continuous, there is large amounts of separation near the rear wheel of the vehicle, although there is some separation due to the body as well. Looking at the Velocity from the top, the effects of the wheels become more apparent. While the Flow around the body has little separation, the flow around the front wheels show large amounts of separation.

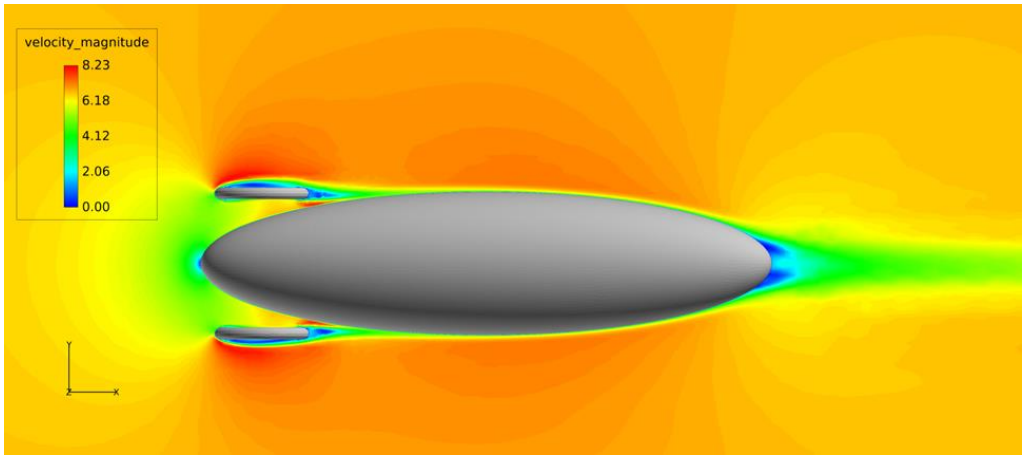

Figure 3.15: Top View of velocity magnitude for wheels out model.

The amount of stagnant flow around the wheels generates a large amount of wake that is comparable, if not larger than the amount of wake near the rear of the body. This are some of the effects that expected to cause the large amount of drag for a vehicle with wheels out. When focusing on the flow around the wheel, it is clear how the flow is greatly affected by the wheel. This is generating large changes in pressure between the front of the rear of the wheel which result in large amounts of drag by the wheels themselves.

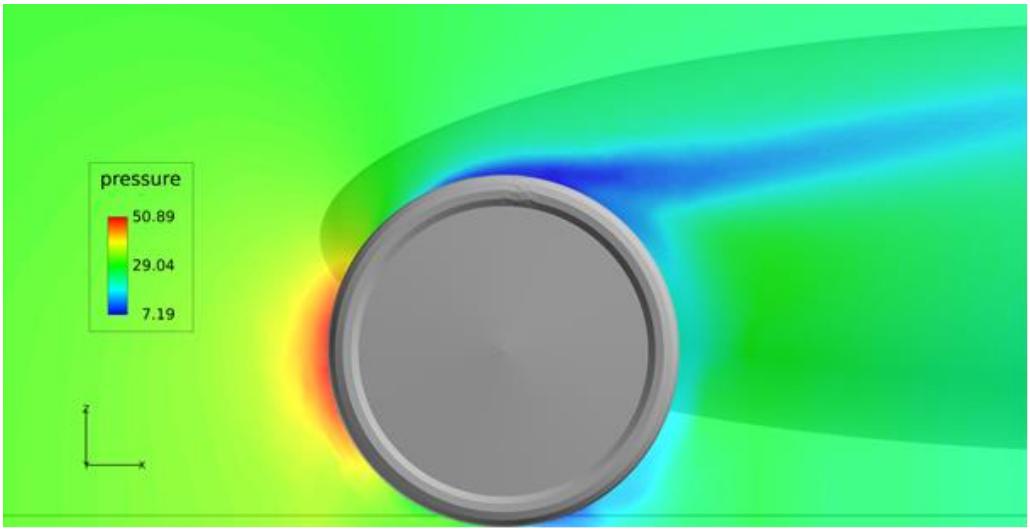

Figure 3.16: Pressure Contour of front wheel.

When comparing the values of rotating wheels, there is considerable difference in the resulting values. This shows the importance of simulating rotating wheels when considering road vehicle applications. The values of drag coefficient for rotating wheels have a difference of about 18%. With values changing from $C_{d,stationary} = 0.318$ to $C_{d,rotating} = .0272$. Looking at the velocity contours for both the stationary and rotating wheel, large differences in the flow can be noted.

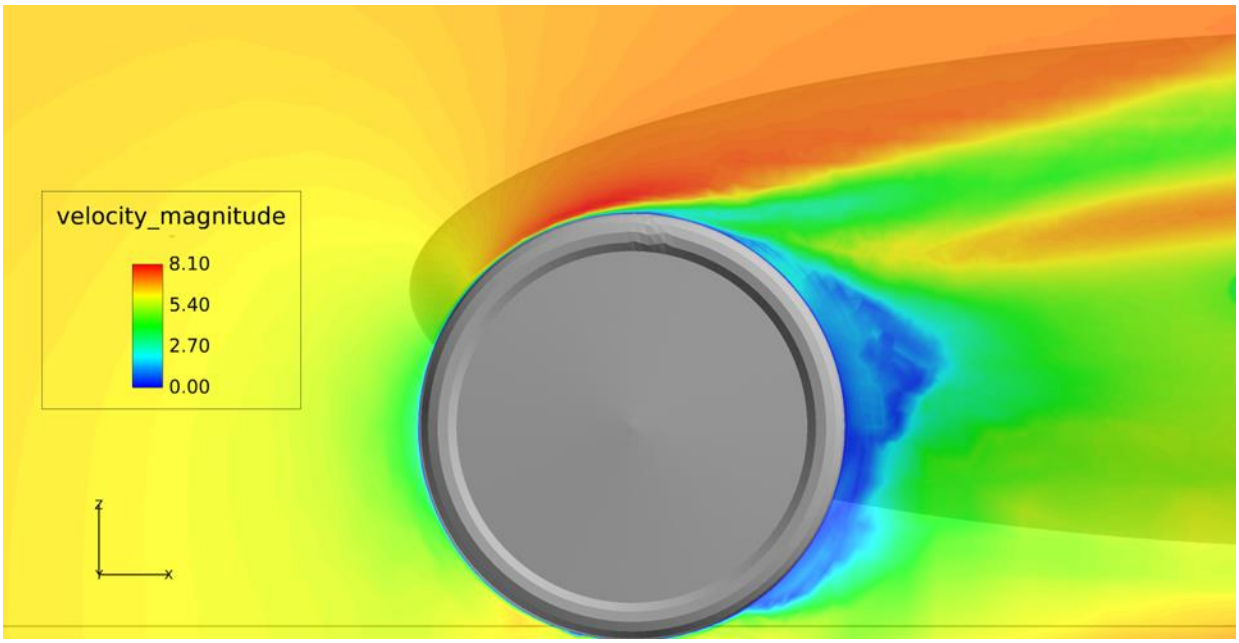

Figure 3.17: Velocity contours of front wheel Stationary

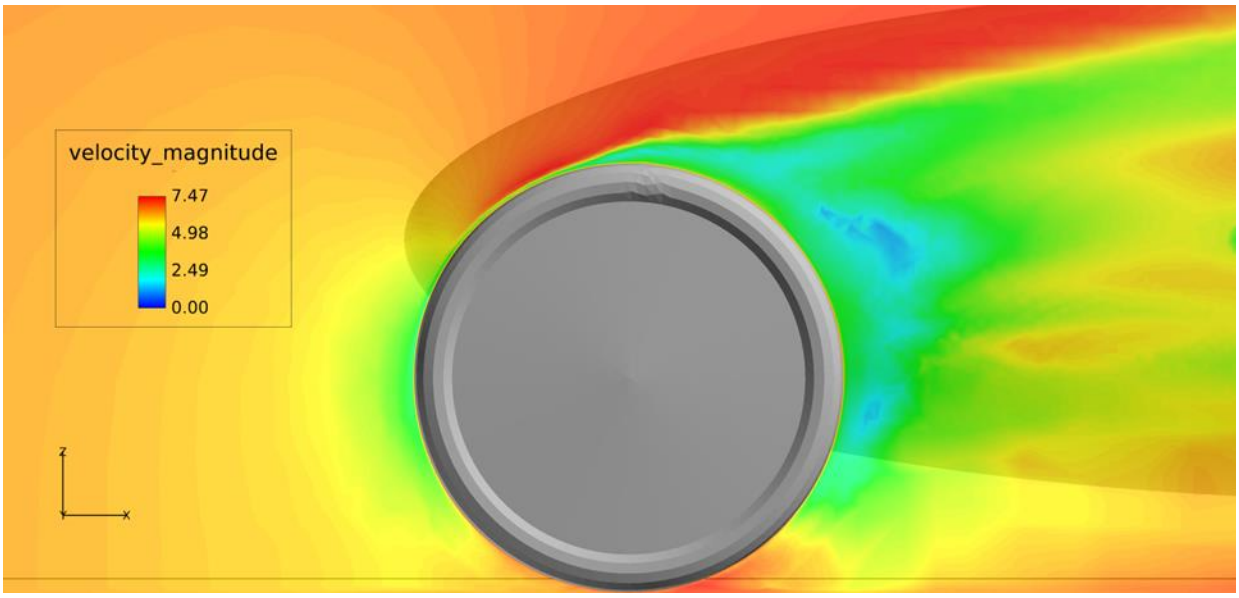

Figure 3.18: Velocity contours of front wheel Rotating

One major difference in the flow is the major reduction in wake behind the wheel. As talked about by W. Hucho, there is a flow of air being pushed out from the front of the wheel

toward the bottom, and jetted toward the back [13]. The wake region is also shifted upward due to the rotation of the wheels and the Magnus effect [2]. This effect also causes a larger amount of higher flowing air to flow above the wheel [2]. While the flow is faster for stationary wheels at 8.10 m/s, the effect is much smaller covering only the top portion of the wheel. Where the fast moving air at 7.47 m/s of the rotating wheel, extends far alongside the body of the vehicle.

When looking at the streamlines focused around the wheel, it is visible how there is a formation of the top vortices. As talked about by A Cogotti, this is caused by the geometry of the wheel, as it behaves as a thin cylinder [10]. The Streamlines of the body show how the flow around the wheels has very significant effects on the flow around the body.

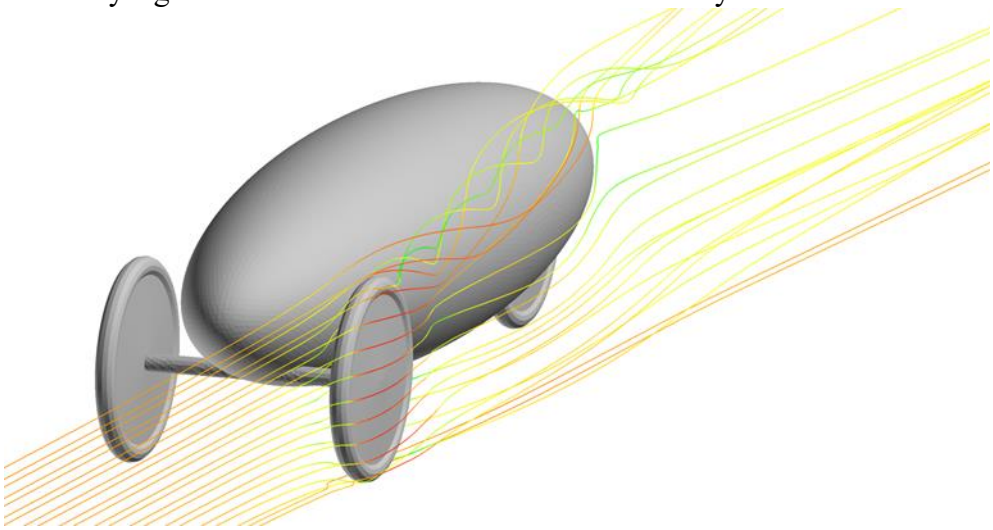

Figure 3.19: Streamlines of flow over stationary wheels

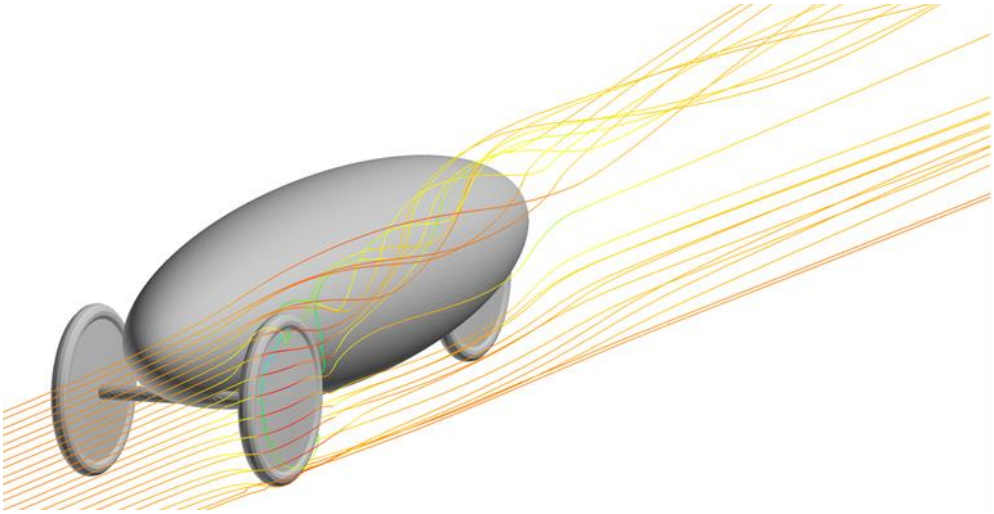

Figure 3.20: Streamlines of flow over rotating wheels.

These effects are further increased when looking at the flow around the rotating wheel. The rotating wheel generates a similar set of vortices. However, as mentioned by W. Hucho, there is flow which guided through the rotation of the wheel into the wake region, which increases the magnitude of the vortex being formed [13].

The resulting drag forces are related to the drag coefficient, there for plotting the drag force against the element size will show a similar convergence to the plot of the drag coefficients. However, the resulting drag force can be compared to the calculated value of drag force of a simple vehicle body with wheels out.

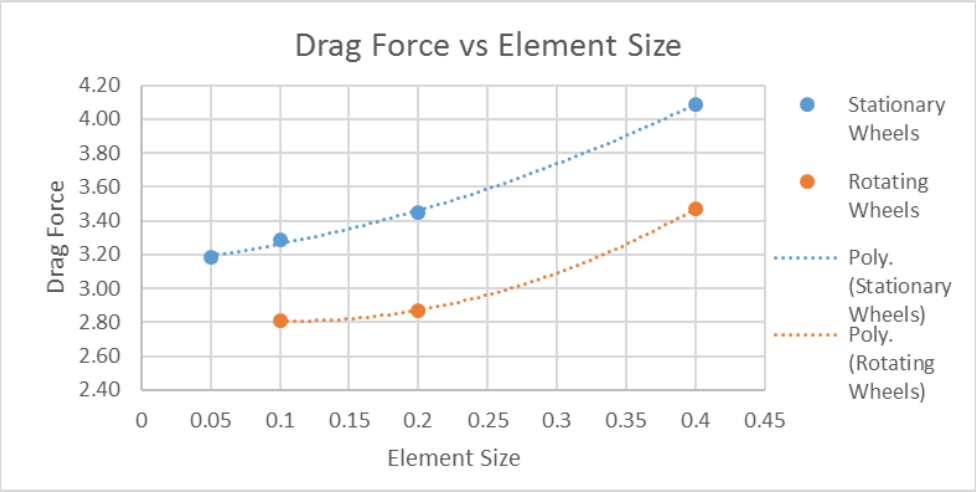

Figure 3.21: Plot of Drag Force vs Element Size

Comparing the Drag force between the two scenarios a considerable decrease in drag by simulating rotating wheels as expected. The value of drag force for a vehicle with stationary wheels is $F_{D,sw} = 3.18\ N$ compared to the value of rotating wheels $F_{D,rw} = 2.81\ N$ which is a difference of 14%. The calculated value for a vehicle with wheels out is $F_{wo} = 2.62\ N$ as shown previously. Although this value neglects the effects of the ground near the vehicle as well as any effects of the rotating wheels.

3.6.2 Results of Wheels In

When looking at the effects of wheels in, there is large differences in the behavior of the air flow when compared to wheels out. While some effects such as the changes in pressure, are more significant, they remain consistent and with less disruption. The resulting values for the drag coefficient of wheels in, is considerably lower than the values of wheels out.

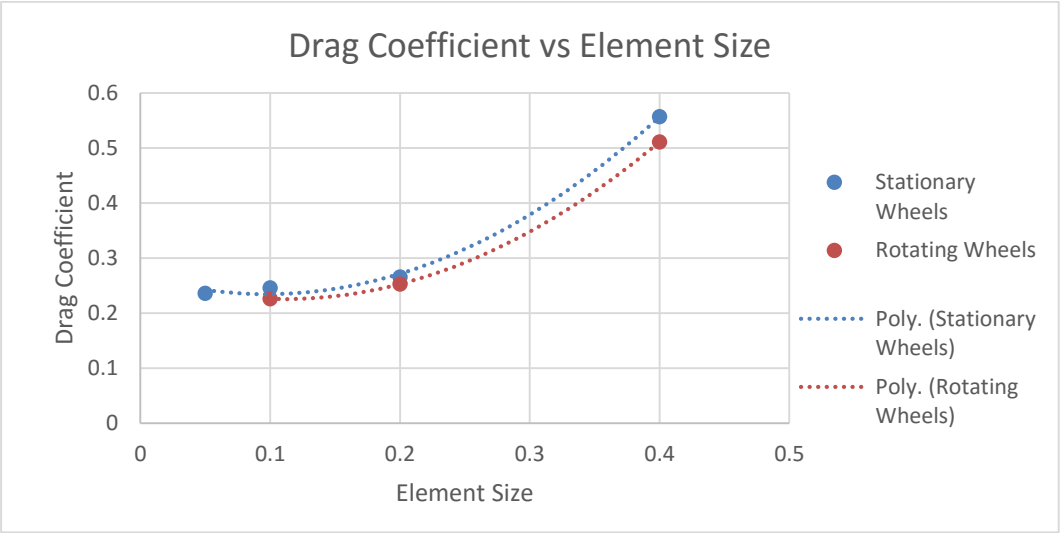

Figure 3.22: Plot of Drag Coefficient against Element Size

More important to note is the relatively smaller difference in results between rotating wheels vs stationary wheels. As expected the covered wheels create less disturbances to the flow of the moving air around the body. Which means that the effects of stationary or rotating wheels has little to no effect on the overall drag of the vehicle.

Looking at the velocity magnitude around the body, it is visible how the velocity of the fluid around the body is higher than before. The velocity at its highest points shows to be 7.79 m/s while for a vehicle with wheels out the highest velocity is 7.54 m/s. While the effects around the body are less significant, the major advantage to this design is projected when looking at the effects around the vehicle's wheels.

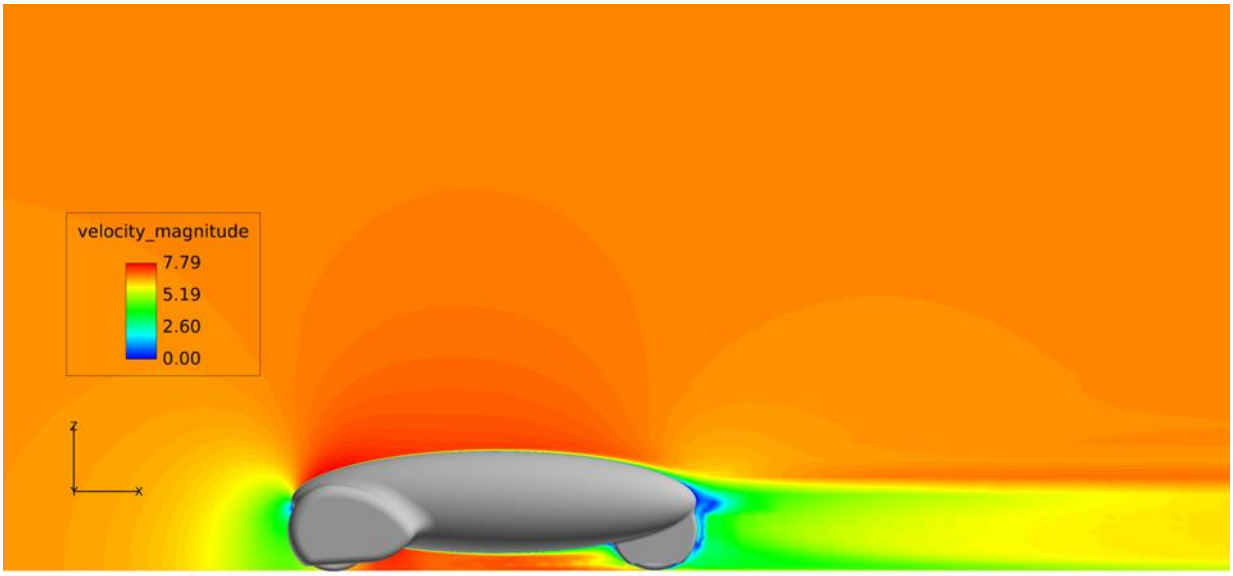

Figure 3.23: Contour of Velocity Magnitude for wheels in

When focusing the velocity magnitude contour around the wheel's geometry, the major differences between wheels in and wheels out begin to show. While the wake region is relatively similar in size when compared to the open wheel, the distribution of the wake is very different. With the majority of the wake being distributed around the top of the fairing around the wheel, the effects of the changes in velocity should cause less of a difference in pressure between the front and back of the wheel. With a lower difference in pressure between the front and the back, it can be expected for the amount of drag to decrease as well. However, the high velocity flow around the top causes a drop in pressure.

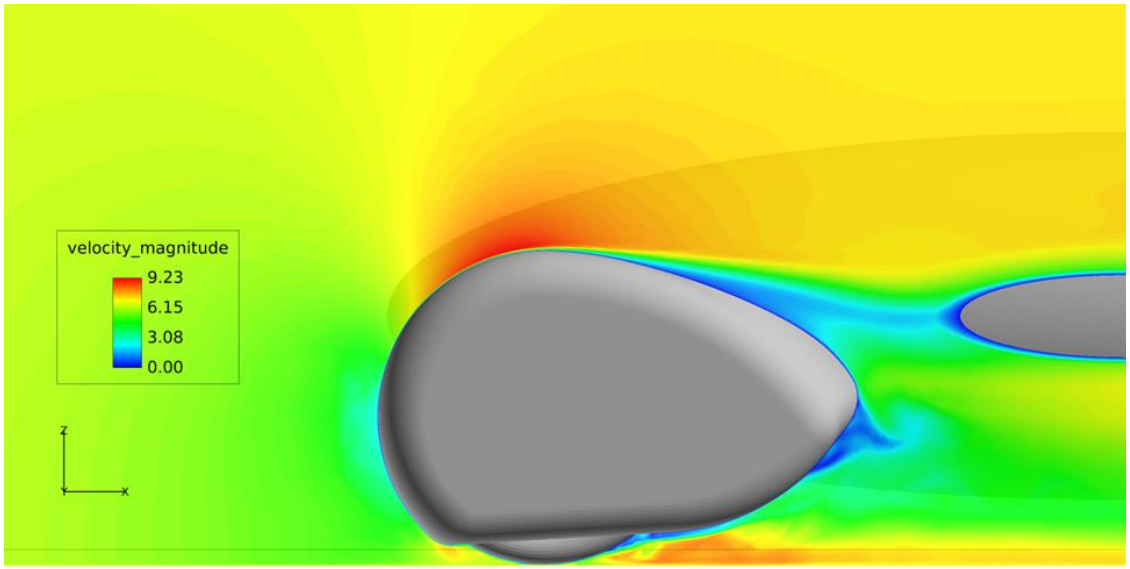

Figure 3.24: Velocity magnitude contour of front wheels for wheels in

This drop in pressure due to the accelerating fluid, results in a pressure drop around the top of the wheel fairing. The pressure drop in the particular area has more of an effect on the vehicles Lift Force than it does to the Drag force.

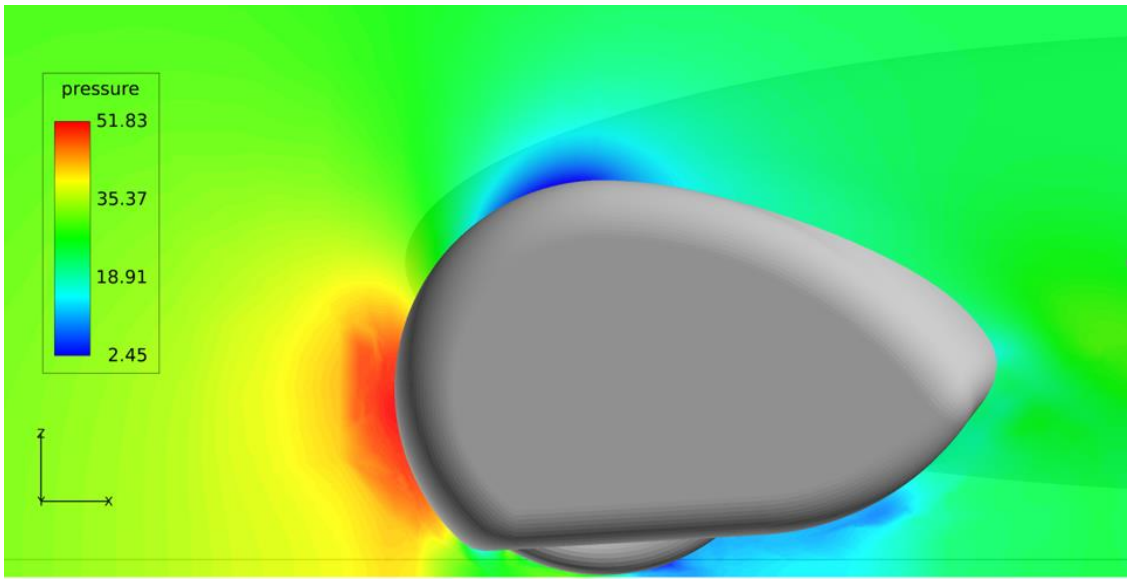

Figure 3.25: Pressure contour for wheels in front wheel.

As mentioned, the flow around the body shows to be much more consistent for wheels in as opposed to wheels out. The velocity contour shows the wake region to be less disrupted, maintaining a much more symmetric wake around the back of the body. Again this is mostly due to the lack of the effects of a rotating wheel. Although, regardless of the effects of rotating wheels being suppressed, there are large increases in frontal area. The large increases in frontal area cause significant increases in the amount of pressure on the front of the vehicle. This leads to the majority of the drag, to be form drag.

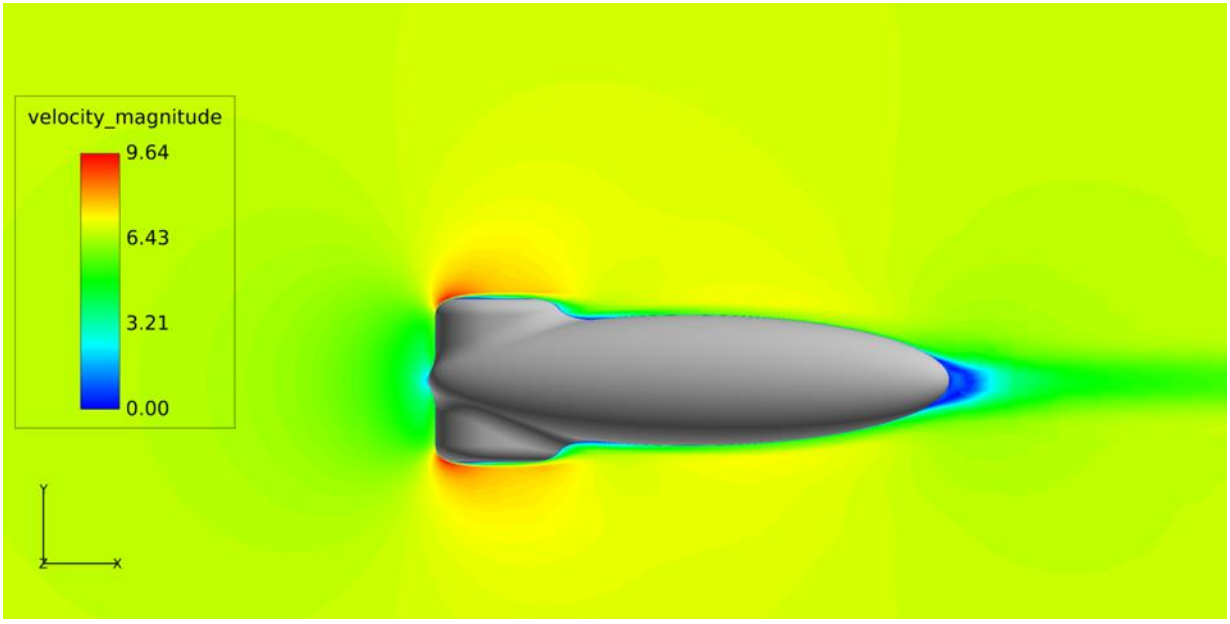

Figure 3.26: Top view of velocity magnitude contour.

Since the amount of wake around the back of the vehicle is larger than that of the vehicle with wheels out, the wheels in model still produces a considerable amount of drag. However, the wheels in model allows for more optimization and refinement of the flow around the body allowing for reductions in drag by reducing separation around the body. This can be much more challenging to attempt on a wheels out model, since there is less control over the behavior of the flow around the wheels

3.7 Conclusion

Comparing the amount of drag produced by both models at different levels of refinement shows how a vehicle with wheels integrated into the body has a lower drag force overall, than a vehicle with open wheels.

The wheels in model resulted in a lower drag coefficient of Cd= 0.226 compared to the wheels out model with a drag coefficient of Cd= 0.272. This difference of 20% becomes less substantial when comparing the drag force. With the larger increase in projected frontal area the total drag force results in 2.75 N of drag force. This compared to the resulting drag force of 2.85N for the wheels out model gives a difference of about 3%. However, there is much more room for improvement of aerodynamics when working with a model with wheels in. These include improved streamlining around the wheels, as well as reduction of frontal area by re-positioning of the front wheels.

Chapter 4: Vehicle Height

4.1 Introduction and Background

While the behavior of air flow over a vehicles body has been well studied and understood, the flow of air underneath has more room for further study. When looking at past studies of flow below the vehicles body, most are simplified. For example, assuming the lower section of a car to be completely smooth. When looking at flow below a vehicles body, there is a larger focus on the effects of lift force as opposed to drag force. While the effects of drag force might be minimal relative to the increases or decreases of lift force, the study will focus on the effects of drag relative to the vehicle height.

4.1.1 Vehicle Nose and Tail

When studying the flow under the vehicle body there is two major factors which have a significant effect on the way the fluid flows under the body. These include the nose of the vehicle as well as the tail of the vehicle. By reducing the height of the vehicle and in turn the stagnation point it is possible to reduce both drag and lift force. This is mostly due to the decrease of air flowing under the vehicle. According to Hucho, having a higher nose can lead to a larger amount of air beneath the vehicle creating a higher pressure leading to a higher lift force [13].

The effects of drag and lift are also largely influenced by the design of the vehicles tail. Although following the geometry of a streamline body is highly desired, it can be highly impractical for many applications. However, mentioned by W. Hucho, the length of the rear end can be decreased with a relatively small effect to the vehicles drag and lift [13]. It is also mentioned that these effects are highly dependent on the tails length as well as the angle of the tapper. The angle of the tapper has to be increased as the length of the tail end of the vehicle decreases [13].

However, if the angle becomes excessively steep, there can be separation of flow much sooner leading to an increase of drag due to the increased wake region.

4.1.2 Ground Effects and Venturi

The desired effect when designing a high performance road vehicle's underbody, is a Venturi nozzle effect. Where the flowing air is accelerated through the bottom of the vehicle in order to reduce the pressure of the fluid underneath. Thus generating greater downforce by creating a pressure differential between the top and the bottom of the vehicle [16]. Early adaptations of these ground effect utilized upside down airfoils, which depended greatly on side skirts to seal the flow of the air through the bottom. In a study by J. Katz it is mentioned how the effects of downforce can be reduced down to 50% with ground clearance of just 20mm for a vehicle using these effects, as shown in the figure 4.1 [14].

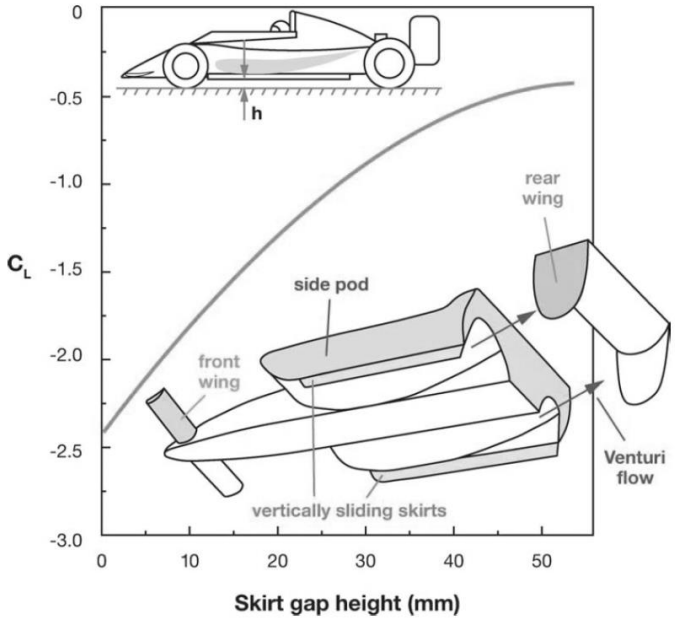

Figure 4.1: Coefficient of lift for ground effect race vehicles [14]

As J. Kats mentions, the effects can be so greatly affected that the design was soon highly restricted by regulations in many racing divisions [14]. Newer designs focusing on generating

Venturi ground effects have been developed such as rear diffusers. The use of a rear diffuser simplifies the design of a vehicles underbody and allows for improved downforce.

Most experiments show how the decrease in ground clearance will cause a drop in the vehicles lift force. W. Hucho states how the decrease in ground clearance will cause the lift force decrease up to a specific point, where the lift force will no longer decrease and begins to increase once more [13]. This maximum point is referred to as the diffuser stall by J. Kats [14]. The Work done by K. R. Cooper on a simplified diffuser at various angles shows the changes of both drag and downforce for various non dimensional ground clearance [15]. Cooper states how the vehicles diffuser stall can be adjusted to different vehicle heights, and by changing the diffusers length and angle the diffuser stall point can be achieved at a higher diffuser angles [15].

The effects of lift force on a vehicles performance, mainly focuses on its traction and stability in most applications, with minimal focus on drag. Since most aerodynamic changes done to improve downforce will often increase the drag of the vehicle [13]. Although Compromising minimal drag for a large increase in vehicle traction, can be acceptable in a high velocity racing vehicle. However, in a high efficiency, high millage vehicle these increases in drag can be more detrimental. This study will focus on the effects of drag relative to the vehicles height.

4.2 Vehicle Modeling

The original wheels out model is modified to adjust for different amounts of ground clearance. The model is adjusted to have a maximum ride height as well as a minimum, without any additional changes to the vehicles aerodynamics. The maximum vehicle height is set to a value before the front axle begins to protrude. The minimum value is then set to a value before the rear wheel begins to protrude out the back through the body. This allows for a ground clearance from 4.50 in to 1.75 in. This difference in height is then split into 6 different cases, with a height difference of .55 in between each.

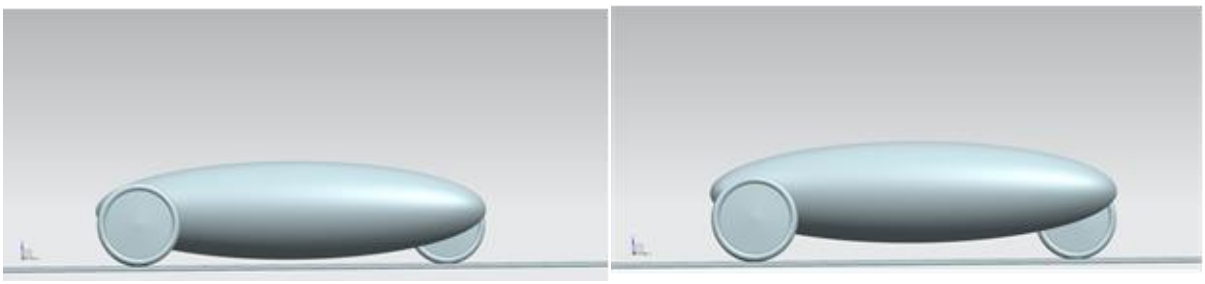

Figure 4.2: Comparison of vehicle ground clearance between minimum and maximum height

One major difference between the two models is the projected frontal area. The decrease in height causes the rear wheel as well as the front axels to be integrated further in the vehicles body, reducing the amount of exposure for these components. As shown by the figure 4.3 the difference in vehicle height causes the frontal area to drop.

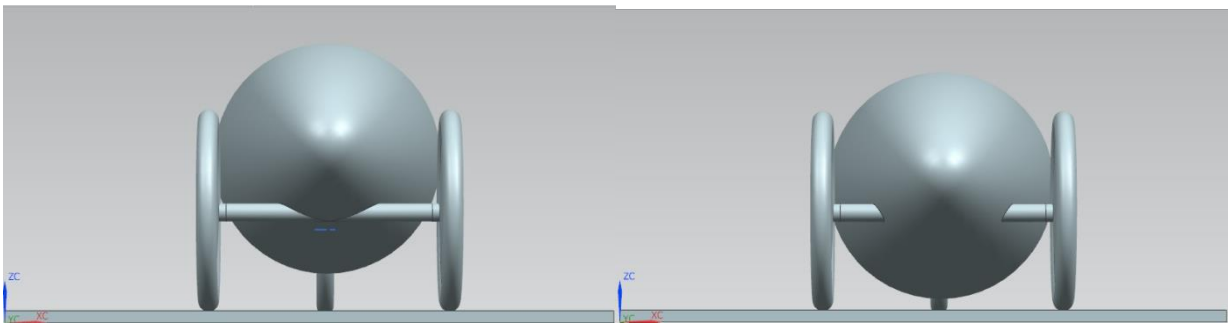

Figure 4.3: Comparison of frontal projected area between maximum and minimum height.

This is shown by the virtual wind tunnel software which shows a difference in frontal area for the different models. With a maximum area of $A_{frontal} = 0.375\, m^2$ for the model with a ground clearance of 4.50 in. and a minimum frontal area of $A_{frontal} = 0.338\, m^2$ for a ground clearance of 1.75 in.

4.3 Model Meshing

All meshing is done using Hypermesh with similar parameters to those done in section 3.3.2 for the wheels out model, in order to maintain consistency through the simulations. Each model generated a mesh with an element size of 1.2 mm for an average mesh size of 62,000

elements. During the meshing process it is important to note that the equivalence parameters for the contact surfaces between the front axle and the wheels requires extra attention when generating the mesh. For each specific model, it is required to delete the axle end caps in order to avoid any overlapping or duplicate elements between the two surfaces.

4.4 Results

Analyzing the velocity contours of the vehicle it is possible to see the changes in velocity due to the change in vehicle height. The following figures show the velocity magnitude contours for the vehicle at its maximum and minimum height.

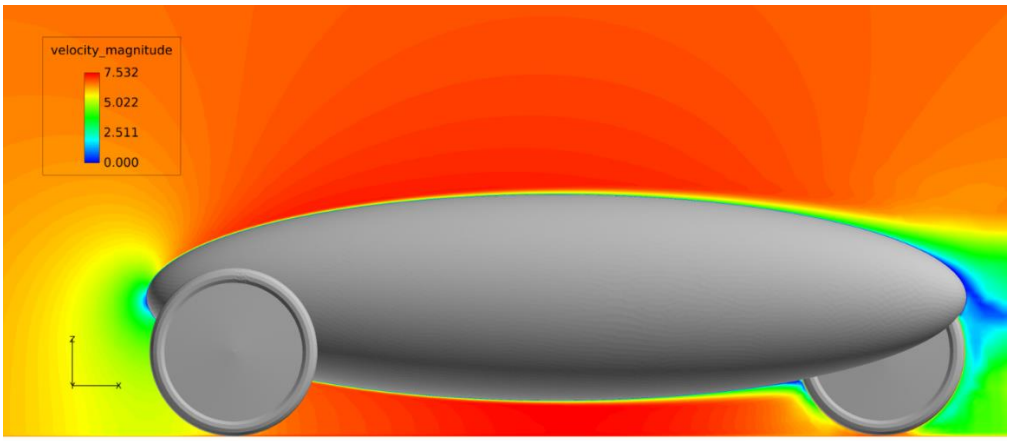

Figure 4.3: Velocity contour of vehicle with maximum ground clearance of 4.50 inches

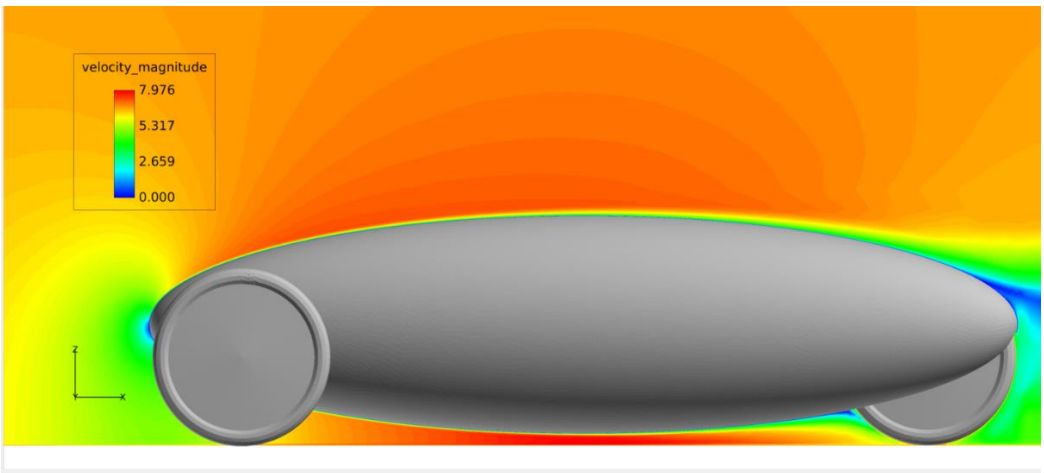

Figure 4.5: Velocity contour of vehicle with minimum ground clearance of 1.75 inches.

The flow of the air going through the bottom of the vehicle begins to increase as the vehicle height is reduced. Observing the contours of the velocity magnitude for the vehicle at maximum ground clearance, the flow appears to be more uniform between the air flowing above the vehicle as well as bellow. As the ground clearance is reduced the difference in velocity between the air flowing above and below the vehicle becomes more significant. The following plots demonstrate these changes in velocity with greater detail. Plotting the velocity magnitude against the distance along the x-axis, it is visible how the increase in pressure initially causes a drop in velocity toward the front of the vehicle between 8 and 9 meters from the front of the wind tunnel. As the flow moves along the body the velocity flows smoothly and quickly around the top and the bottom of the vehicle with a drop in velocity peaking at 10 meters. This flow then slows down again as the air reaches the rear of the vehicle, followed by a sudden disruption caused by the rear wheel at around 11 meters. The flow then continues to flow into the wake region.

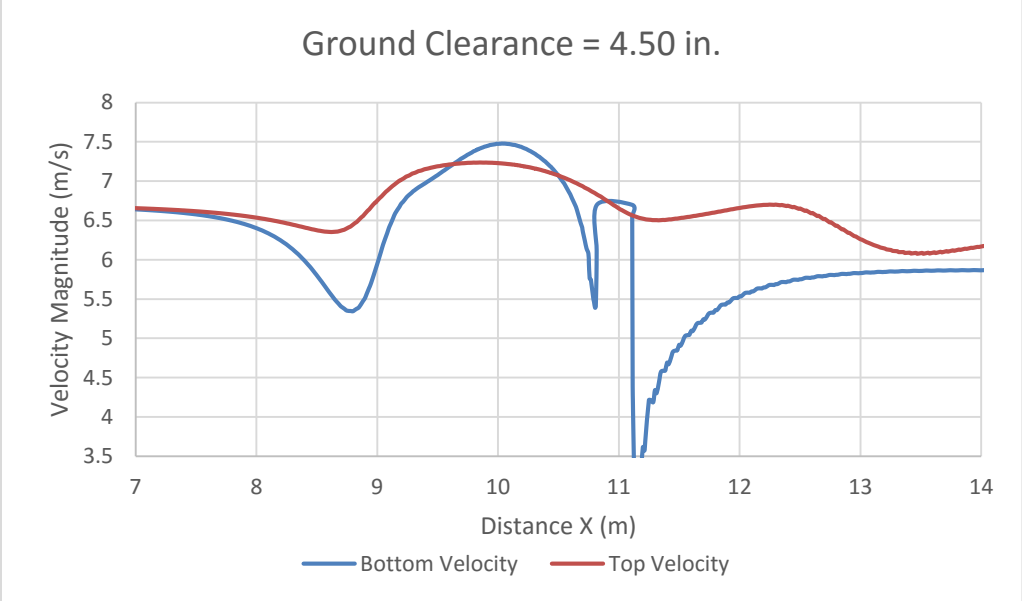

Figure 4.6: Velocity Plot for distance X of Ground Clearance 4.50

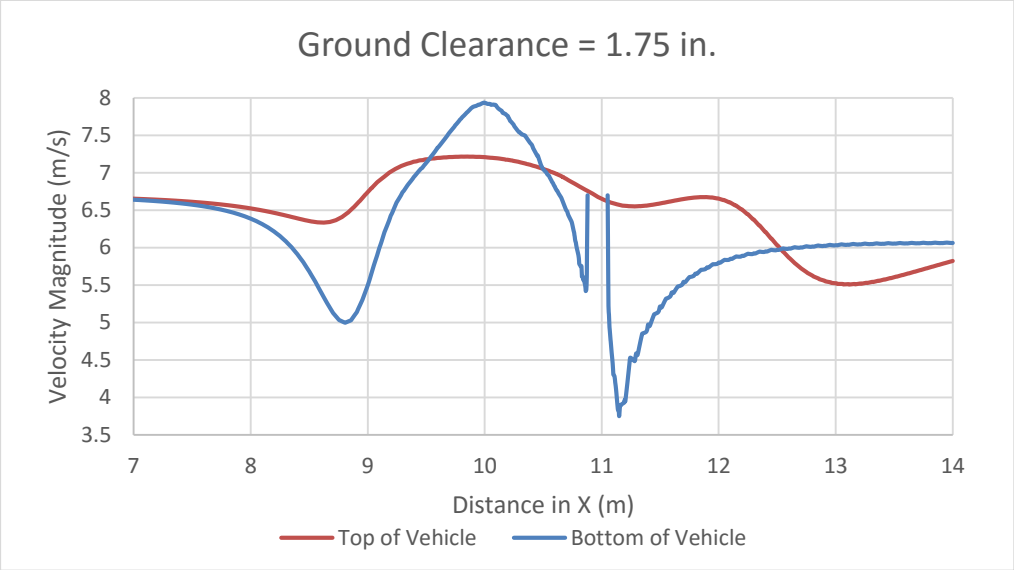

Figure 4.7: Velocity plot for distance X of Ground Clearance 1.75in

As shown by the plots, the difference in velocity between the top and the bottom for a vehicle of 4.50in. in ground clearance is much smaller, at just 7.23 m/s for the top velocity and 7.47 m/s for the bottom velocity. While the difference for a ground clearance of 1.75 m/s results in a velocity of 7.21 m/s for the top and 7.93 m/s for the bottom.

As expected the resulting Lift force drops as there is a decrease in vehicle height. There is also an increase in the drag coefficient, however the amount of drag force calculated results in a decrease.

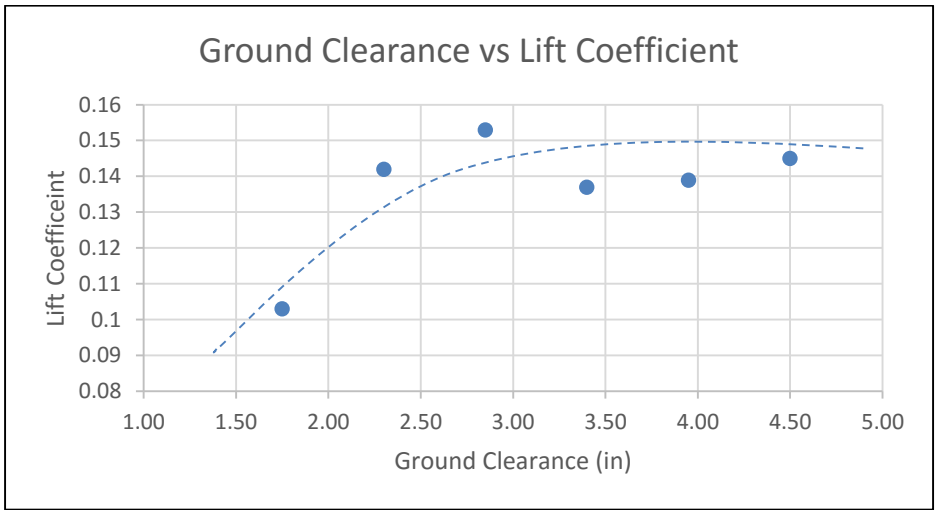

Figure 4.8: Lift Coefficient of vehicle against Ground Clearance

As shown by the plot, the Lift force fluctuates initially as the vehicle height is decreased. This is then followed by a very large decrease in the lift force when reaching a vehicle height bellow 2.50 in. in ground clearance. This is most likely due to the Venturi effect beginning to propagate after the height is lowered beyond that point. According to J. Katz a further decrease in ground clearance would begin to cause an increase in lift force [14]. Although this is not visible in the previous plot, it does follow the behavior expected when compared to the J. Katz study. It is mentioned by Katz when looking at a simple rear diffuser, the stall point will occur at a H/L = .02 for a diffuser angle of 10 degrees [14].

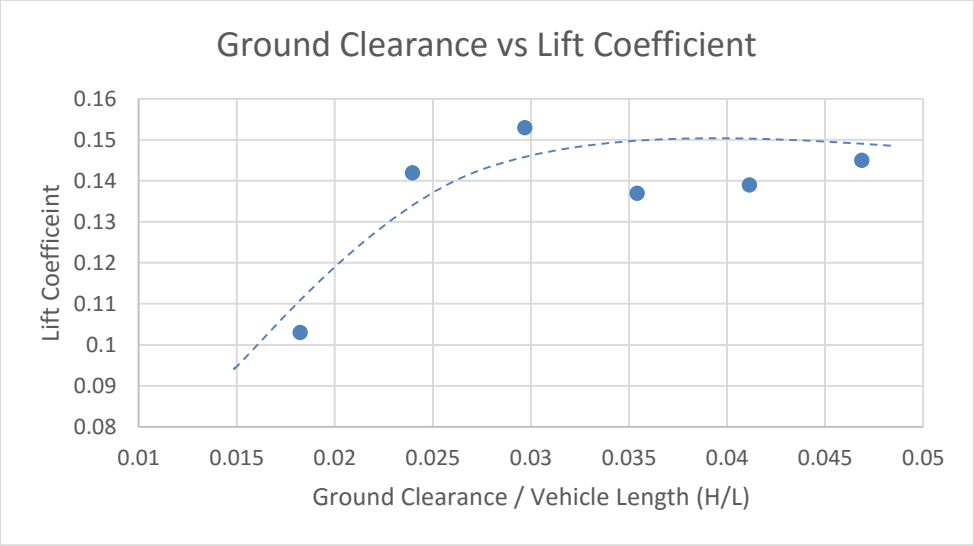

Figure 4.9: Lift Coefficient of vehicle against ratio H/L

When plotting the resulting lift coefficient against the vehicles H/L, it appears that a diffuser stall point begins to occur between the H/L values of .015 and .02. The deviation from the value stated by J. Katz is mostly due to the difference in the diffuser angle, where the angle is set to 10 degrees, as well as the rounded geometry of the vehicle model used in this case.

When focusing on the effects of drag, the ground clearance has a relatively smaller change when compared to the changes in lift. While there is a drop of $\Delta C_l = 0.05$ from its highest value to its lowest, the increase in drag coefficient is $\Delta C_d = 0.02$.

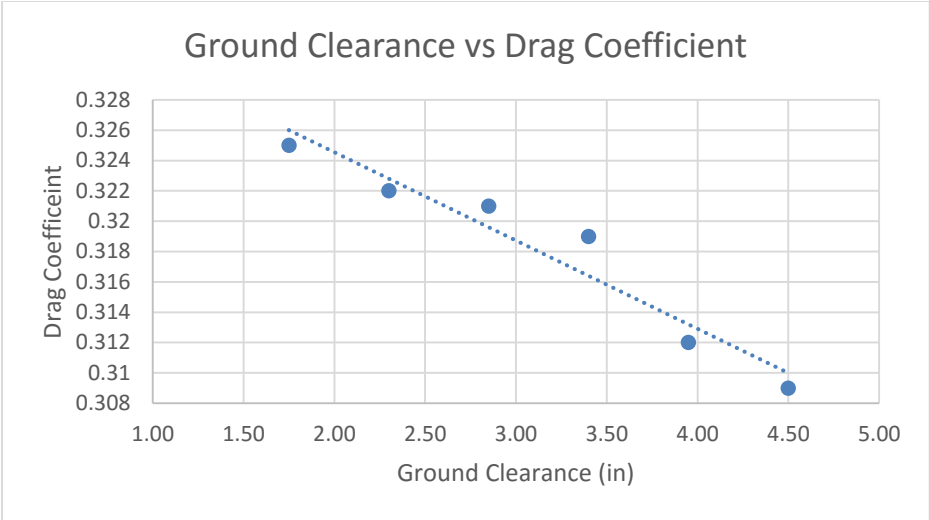

Figure 4.10: Drag Coefficient relative to ground clearance.

Although the drag coefficient increases as the ground clearance is decreased the change in frontal area has a more profound effect on the total drag force. When plotting the resulting drag force against the ground clearance there is a drop in the total drag force of the vehicle.

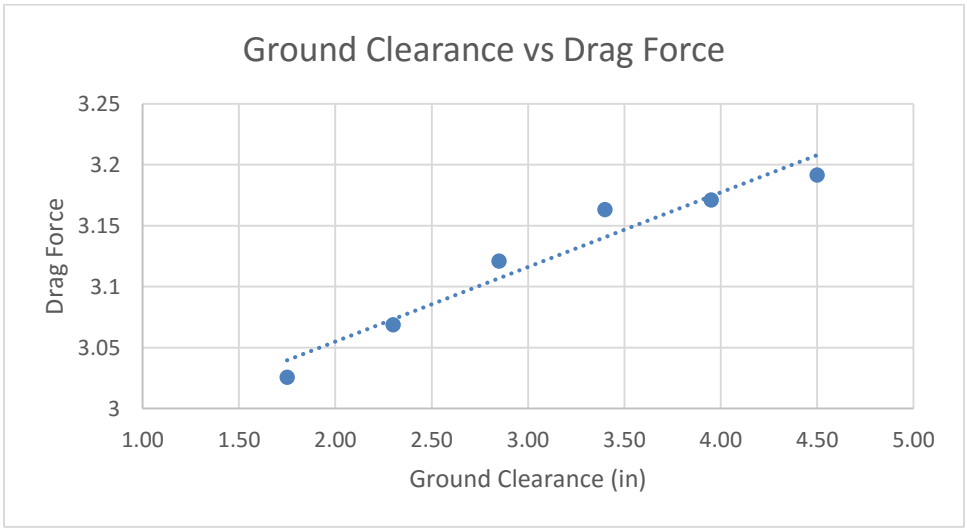

Figure 4.11: Drag Force against ground clearance.

With a drag coefficient increase of $\Delta C_d = 0.02$, the drag force is more affected by the frontal area decrease of $\Delta A_{frontal} = 0.04\, m^2$. One other major consideration for the decrease in total drag force is the reduced effects of the rear wheel. As established in Chapter 3 the geometry and the rotation of a vehicles wheels cause a large increase in the drag force. By decreasing the vehicle height, the rear wheel sits further within the body of the vehicle. This can lead to decreases in drag force due to the lower exposure of the rear wheel to the flowing air.,

4.5 Conclusion

The results show the decreases in lift force and drag force are minimal with the changes in vehicle ground clearance. While a decrease in lift force is beneficial for vehicle handling, the generated forces are negligible at the current velocity used. Although, the increases in drag coefficient are of importance in this application, the decrease in frontal surface area causes the resulting drag force to reduce despite the increase. Based on the current results the decrease in ground clearance may be beneficial due to the decrease in drag force as well as the decrease in lift force. However, a further study of the effects of ground clearance should be considered.

References

[1][Shell Global. (2016). Shell Eco-marathon. Retrieved April 18, 2016, from http://www.shell.com/energy-and-innovation/shell-ecomarathon.html]

[2][Çengel, Y. A., & Cimbala, J. M. (2006). Fluid mechanics: Fundamentals and applications. Boston: McGraw-HillHigher Education.]

[3][Hibbeler, R. C. (2015). Fluid mechanics, global edition. Place of publication not identified: Pearson Education Limited.]

[4][Wendt, J. , Governing Equations of Fluid Mechanics in Computational Fluid Dynamics an Introduction, 3rd ed., Springer,Berlin, 2009.]

[5][Tu, J., Inthavong, K., & Ahmadi, G. (2013). Computational fluid and particle dynamics in the human respiratory system. Dordrecht: Springer.]

[6][Spalart, P. R., & Allmaras, S. R. (1992). A one-equation turbulence model for aerodynamic flows.]

[7][Celik, I., Chen, C., & Roache, P. (1993). Quantification of uncertainty in computational fluid dynamics: Presented at the Fluids Engineering Conference, Washington, DC, June 20-24, 1993. New York: American Society of Mechanical Engineers]

[8][TACC. (2016). User Portal. Retrieved April 18, 2016, from https://portal.tacc.utexas.edu/user-guides/lonestar5]

[9][Shell Global. (2016). SHELL ECO-MARATHON 2016 OFFICIAL RULES CHAPTER I. Retrieved April 18, 2016, from http://s06.static-shell.com/content/dam/shell-new/local/corporate/ecomarathon/downloads/pdf/global/sem-2016-global-rules-chapter1-010715.pdf.]

[10][Cogotti, A. (1983). Aerodynamic Characteristics for Car Wheels. Int. Jounral of Vehicle Design, SP 3, 173-196]

[11][Mercker, E., & Knape, H. (1989). Ground Simulation with Moving Belt and Tangential Blowing for Full-scale Automotive Testing in a wind Tunnel. SAE Technical Paper Series. doi:10.4271/890367]

[12] [Hucho, W. -. (1978). The Aerodynamic Drag of Cars Current Understanding, Unresolved Problems, and Future Prospects. Aerodynamic Drag Mechanisms of Bluff Bodies and Road Vehicles, 7-44. doi:10.1007/978-1-4684-8434-2_2

[13][Hucho, W. (1998). Aerodynamics of road vehicles: From fluid mechanics to vehicle engineering. Warrendale, PA: Society of Automotive Engineers.

[14][Katz, J. (2006). Aerodynamics Of Race Cars. Annu. Rev. Fluid Mech. Annual Review of Fluid Mechanics, 38(1), 27-63. doi:10.1146/annurev.fluid.38.050304.092016

[15][Cooper, K. R., Bertenyi, T., Dutil, G., Syms, J., & Sovran, G. (1998). The Aerodynamic Performance of Automotive Underbody Diffusers. SAE Technical Paper Series. doi:10.4271/980030

[16][Katz, J. (1996). Race car aerodynamics: Designing for speed (2nd ed.). Cambridge, MA, USA: R. Bentley]

[17][Wiedemann, J. (1996). The influence of ground simulation and wheel rotation on aerodynamic drag optimization: Potential for reducing fuel consumption. Warrendale, PA: Society of Automotive Engineers]

Appendix

Acusolve.cnf

The .cnf file specifies parameters for the acusolve code, and is

```
$acusolve settings
acuRun.host_lists                     = _auto
acuRun.num_threads                    = _auto
acuRun.message_passing_type           = impi
acuRun.view_message_passing_type      = impi
acuRun.num_processors_per_node        = 24
```

Job pre-processing script

This script is used to do all pre-processing of the simulation after files have been uploaded to server.

```
#!/bin/bash
#SBATCH -J myMPI            # job name
#SBATCH -o myMPI.o%j        # output and error file name (%j expands to
jobID)
#SBATCH -N 1                # number of nodes requested
#SBATCH -n 24               # total number of mpi tasks requested
#SBATCH -p development      # queue (partition) -- normal, development, etc.
#SBATCH -t 01:30:00         # run time (hh:mm:ss) - 1.5 hours

export ALTAIR_LICENSE_PATH=6200@129.108.156.61

/work/03886/cmata101/lonestar/altair/13.0/altair/acusolve/linux64/plugins/bin
/acuVwt /work/03886/cmata101/lonestar/simulations/sim1/ vwtAnalysis sub 24


cp ~/jobscriptsolve.txt /work/03886/cmata101/lonestar/simulations/sim1/
```

Job Solving script

This code is used to solve the simulation which has been pre-processed.

```
#!/bin/bash
#SBATCH -J myMPI            # job name
```

```
#SBATCH -o myMPI.o%j       # output and error file name (%j expands to
jobID)
#SBATCH -N 2               # number of nodes requested
#SBATCH -n 48              # total number of mpi tasks requested
#SBATCH -p normal          # queue (partition) -- normal, development, etc.
#SBATCH -t 05:30:00        # run time (hh:mm:ss) - 1.5 hours

export ALTAIR_LICENSE_PATH=6200@129.108.156.61

acuRun -dir ACUSIM.DIR -pb vwtAnalysis -inp vwtAnalysis.inp -np 48 -nt 24 -do

solve -slurm
```

Force Budget Matlab Code

This code is used to calculate the total losses on a shell eco marathon vehicle

```
%**************************************************************************
%**
%**  Friction force model for the Shell-Eco Marathon vehicle.
%**
%**         By Jack Chessa (jfchessa@utep.edu)
%**
%**  This is a fairly simple model to use. It employs some rather "back of
%**  the envelop" calculations to determine the approximate friction
%**  forces for a vehicle.  These can then give an estimate on the vehicle
%**  fuel efficiency.
%**
%**
%**************************************************************************

%-----------------------  MODEL INPUT PARAMETERS -------------------------%
MPG=3000;    % target mpg

% Vehicle parameters
VehicleWeight = 80; %[lbm]
DriverWeight = 90;  % driver weight [lbm]
SpeedLow=12;        % engine on speed [mph] (currently does not affect the model)
SpeedHigh=18;       % engine off speed [mph]

% motor parameters
EngineEff=0.20;     % ic engine efficency
TorqueMotor=1;      % engine torque [N-m] Honda GXH25
RpmMotor=5000;      % engine rpm [RPM]

% tire parameters Michelin 45-75R16 tire (the blue ones)
WheelDia=16; % [in]
CoeffRollingFriction=.00081;  % tire rolling coefficient of friction
TurningCoef=10*CoeffRollingFriction;
TurningPercent=.15;           % percent of course where turning

BearingDia=1.5;             % wheel bearing mean diameter [in]
BearingFrictionCoef=0.002;  % coefficient of friction of the wheel bearing
```

```
% aerodynamic parameters
FairingHeight=24;   % [in]
FairingLength=8*12; % [in]
FairingWidth=30;    % outer fairing dimensions [in]
TurbulentFlag=0;    % forces the calculation to assume turbulent

%-------------------- END OF MODEL INPUT PARAMETERS ----------------------%
%  DO NOT TOUCH ANYTHING BELOW THIS LINE
%  UNLESS YOU UNDERSTAND THE MODELS AND WISH TO CHANGE THEM.

fprintf('\n\n*****************************************************************\n');
fprintf('**                                                             **\n');
fprintf('**       Shell Eco-Marathon Vehicle Design Model               **\n');
fprintf('**                                                             **\n');
fprintf('*****************************************************************\n');
fprintf('\n\n               D E S I G N     S U M M A R Y\n\n');
fprintf('  Weight of vehicle:                          %6.1f lbm\n',VehicleWeight);
fprintf('  Weight of driver:                           %6.1f lbm\n',DriverWeight);
WeightVehicleDriver=VehicleWeight+DriverWeight; % total weight of vehicle and driver
[lbm]
fprintf('  Weight of vehicle with driver:              %6.1f
lbm\n',WeightVehicleDriver);
fprintf('  Lower limit of vehicle speed:               %6.1f mph\n',SpeedLow);
fprintf('  Upper limit of vehicle speed:               %6.1f mph\n',SpeedHigh);
fprintf('  Average vehicle speed:                      %6.1f
mph\n',SpeedHigh/2+SpeedLow/2);
fprintf('  Engine efficiency:                          %6.0f %%\n',EngineEff*100);
fprintf('  Engine torque:                              %6.1f N-m\n',TorqueMotor);
fprintf('  Engine RPM:                                 %6.0f rpm\n',RpmMotor);
fprintf('  Drive wheel diameter:                       %6.1f in\n',WheelDia);
fprintf('  Tire rolling friction coefficient (straight): %6.4f
lbm\n',CoeffRollingFriction);
fprintf('  Tire rolling friction coefficient (in turn):  %6.4f lbm\n',TurningCoef);
fprintf('  Percent of course in turn:                  %6.0f
%%\n',100*TurningPercent);
fprintf('  Wheel bearing diameter:                     %6.2f in\n',BearingDia);
fprintf('  Bearing rolling coefficent:                 %6.4f
\n',BearingFrictionCoef);
fprintf('  Height fairing:                             %6.1f in\n',FairingHeight);
fprintf('  Length of fairing:                          %6.1f in\n',FairingLength);
fprintf('  Width of fairing:                           %6.1f in\n',FairingWidth);
if ( TurbulentFlag==1 )
    fprintf('  Turbulent flow assumed:                        yes\n');
else
    fprintf('  Turbulent flow assumed:                         no\n');
end

%============= calculations section ================

MassTotal=WeightVehicleDriver*(0.45359); % total mass [kg]
WeightTotal=WeightVehicleDriver*(4.44822); % total weight [N]

ForceBudget=EngineEff*19873/MPG; % Total allowable drag force [N]

VelocityLow=SpeedLow*(0.44704); % [m/s]
VelocityHigh=SpeedHigh*(0.44704); % [m/s]
VelocityMean=(VelocityLow+VelocityHigh)/2;

WheelDia=WheelDia*(0.0254); % [m]
WheelRPM=19.1*VelocityMean/WheelDia; % [rpm]
GR=RpmMotor/WheelRPM; % gear reduction in transmission from motor to wheel
```

```
TorqueWheel=TorqueMotor*GR; % torque applied to the wheel from transmission [N-m]
ForceMotor=TorqueWheel*(2/WheelDia); % force of the motor on the vehicle [N]

fprintf('\n\n   C A L C U L A T E D     D E S I G N     P A R A M E T E R S  \n\n');
fprintf('  Wheel rpm:                                    %6.1f rpm\n',WheelRPM);
fprintf('  Gear reduction:                              %6.1f:1\n',GR);
fprintf('  Torque at wheel:                              %6.1f N-m\n',TorqueWheel);

fprintf('\n\n           D R A G      F O R C E      S U M M A R Y\n\n');

%-------------------------------------------------------------------------------
-------
ForceRolling=WeightTotal*CoeffRollingFriction; % force on vehicle due to rolling
resistance
                                               % of tires
fprintf('  Rolling drag force:                           %6.1f N\n',ForceRolling);

%-------------------------------------------------------------------------------
-------
BearingDia=BearingDia*(0.0254); % [m]
ForceBearings=WeightTotal*BearingFrictionCoef*BearingDia/WheelDia;
fprintf('  Bearing drag force:                           %6.1f N\n',ForceBearings);

%-------------------------------------------------------------------------------
-------
FairingHeight=FairingHeight*(0.0254); % [m]
FairingLength=FairingLength*(0.0254); % [m]
FairingWidth=FairingWidth*(0.0254); % [m]
FrontalArea=FairingWidth*FairingHeight;
AirViscosity=1.53e-5; % kinematic viscosity of air [m^2/s]
AirDensity=1.18 ; % density of air [kg/m^3]
if ( TurbulentFlag==1 )
    ReTrans=0;
else
    ReTrans=3.2e5;
end

Re=VelocityMean*FairingLength/AirViscosity; % Reynolds number
AspectRatio=FairingLength/sqrt(FrontalArea);

% interpolate drag coefficeints (Shames "Mechanics of Fluids" Table 10.2)
if ( Re>ReTrans ) % turbulent
    Cd=interp1([1,2,4,8],[.27,.06,.06,.13],AspectRatio);
    fprintf('  Reynolds number:                                %6.0f (turbulent)\n',Re);
else % laminar
    Cd=interp1([1,2,4,8],[.47,.27,.2,.25],AspectRatio);
    fprintf('  Reynolds number:                                %6.0f (laminar)\n',Re);
end

ForceFormDrag=Cd*FrontalArea*0.5*AirDensity*VelocityMean^2;

% Separation??

fprintf('  Vehicle aspect ratio:                        %6.2f:1 \n',AspectRatio);
fprintf('  Drag coefficient:                             %6.2f \n',Cd);
fprintf('  Form drag force:                              %6.1f N\n',ForceFormDrag);

%-------------------------------------------------------------------------------
-------
% skin friction coefficent calculations from (Shames "Mechanics of Fluids" Table 10.1)
```

```
A=interp1([3e5,5e5,1e6,3e6],[1050,1700,3300,8700],Re);
Cf = 0.074/Re^(1/5) - A/Re;
FairingSurfaceArea=2*(FairingWidth+FairingHeight)*FairingLength+2*FrontalArea;
ForceSkinDrag=Cf*FairingSurfaceArea*0.5*AirDensity*VelocityMean^2;
fprintf('  Skin drag force:                              %6.1f N\n',ForceSkinDrag);

%-------------------------------------------------------------------------------------------
-------
ForceTurning= TurningPercent*TurningCoef*WeightTotal;
fprintf('  Turning drag force:                           %6.1f N\n',ForceTurning);

%-------------------------------------------------------------------------------------------
-------
ForceCoast=ForceSkinDrag+ForceFormDrag+ForceBearings+ForceRolling;
DeltaVel=VelocityHigh-VelocityLow;
DistCoast=MassTotal*DeltaVel^2/(2*ForceCoast);
DtCoast=MassTotal*DeltaVel/(ForceCoast);

EtaAccel=ForceCoast/ForceMotor;
ForceAccelActual=(ForceMotor-ForceCoast);
ForceAccel=EtaAccel*ForceAccelActual;
fprintf('  Acceleration drag force:                      %6.1f N\n\n',ForceAccel);

%-------------------------------------------------------------------------------------------
-------
DtAccel=MassTotal*DeltaVel/ForceAccelActual;
DistAccel=MassTotal*DeltaVel^2/(2*ForceAccelActual);

ForceTotal=ForceCoast+ForceAccel;
DesignMPG=EngineEff*19873/ForceTotal; % MPG for the design

%-------------------------------------------------------------------------------------------
-------
pie([ForceRolling,ForceBearings,ForceFormDrag,ForceSkinDrag,ForceTurning,ForceAccel])
legend('Rolling','Bearings','Form Drag','Skin Drag','Turning','Accel')
title(['Force Budget For Eco-Marathon Vehicle, F_{Total}=',num2str(ForceTotal,2),' N,
Projected MPG=',num2str(DesignMPG,4)])


fprintf('  Total drag force:                             %6.1f N\n',ForceTotal);
fprintf('  Budgeted drag force:                          %6.1f N\n',ForceBudget);
fprintf('  Model MPG:                                    %6.0f mpg\n',DesignMPG);

fprintf('\n\n     C O A S T     A N D     K I L L     S U M M A R Y\n\n');
fprintf('  Engine force:                                 %6.1f N\n',ForceMotor);
fprintf('  Coasting drag force:                          %6.1f N\n',ForceCoast);
fprintf('  Coasting power:                               %6.1f
W\n',ForceCoast*VelocityMean );
fprintf('  Coasting power:                               %6.3f
hp\n',ForceCoast*VelocityMean*0.00134102209 );
fprintf('  Coast time:                                   %6.1f sec\n',DtCoast);
fprintf('  Acceleration time:                            %6.1f sec\n',DtAccel);
fprintf('  Coast distance:                               %6.1f m\n',DistCoast);
fprintf('  Acceleration distance:                        %6.1f m\n',DistAccel);
fprintf('  Percent distance accelerating:                %6.1f
%%\n',100*DistAccel/(DistAccel+DistCoast));


fprintf('\n\n************************************************************\n');
```

Richardson Extrapolation Code

This code is used to calculate the Richardson extrapolation

Richardson Extrapolation with determination of mesh error estimate as well as convergence rate

A is the value of interest in your computation and h is the characteristic element size. You need these at three different meshes: h0, h1, h2 and A0, A1 and A2

Input values

```
h0 = 1.0;
h1 = 0.5;
h2 = 0.25;
A0 = 2.2;
A1 = 2.0;
A2 = 1.95;
```

Solve for the convergence rate, α and the value at h -> 0, A

```
e0 = A == A0 + a h0^α
e1 = A == A1 + a h1^α
e2 = A == A2 + a h2^α
```

```
A == 2.2 + 1. a
```

```
A == 2. + 0.5^α a
```

```
A == 1.95 + 0.25^α a
```

```
sol = NSolve[{e0, e1, e2}, Reals]
```

```
NSolve::ratnz: NSolve was unable to solve the system with inexact coefficients.
    The answer was obtained by solving a corresponding exact system and numericizing the result. >>
{{a → -0.266667, A → 1.93333, α → 2.}}
```

Estimate the descritization error

The way to report the answer is A2 ± err

```
err = A2 - (A) /. sol[[1]]
```

```
0.0166667
```

Just check the fit. Set k to the real part of α with C[1]=0

```
Show[Plot[(A - a h^α) /. sol, {h, 0, 1.0}], ListPlot[{{h0, A0}, {h1, A1}, {h2, A2}}] ]
```

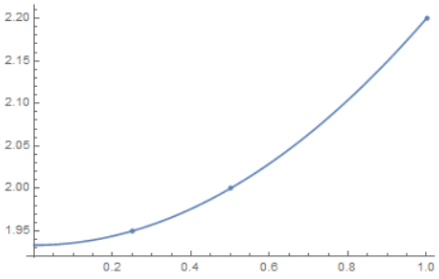

Simulation results for sphere validation

Sphere	Diar	Front	Veloc	Dens	With	Height	Length	W/D ratio	Far F	Near	buff	BL height	Layer	# of Ele	Drag Coe	Lift Coef	Drag Force
4446	2.286	4.23	6.7056	1.225	10	10	25	4.374453193	0.2	0.02	10	0.00252	2	405879	0.11012	-0.01947	12.82885658
4446	2.286	4.23	6.7056	1.225	10	10	25	4.374453193	0.2	0.02	10	0.00252	4	451020	0.12111	-0.04454	14.10917927
4446	2.286	4.23	6.7056	1.225	10	10	25	4.374453193	0.2	0.02	10	0.00252	8	542361	0.25912	0.12025	30.18718959
4446	2.286	4.23	6.7056	1.225	10	10	25	4.374453193	0.2	0.02	10	0.00252	16	643090	0.28443	-0.05268	33.13577623
4446	2.286	4.23	6.7056	1.225	10	10	25	4.374453193	0.2	0.02	10	0.00252	24	653116	0.28262	0.01628	32.92491326
4446	2.286	4.23	6.7056	1.225	10	10	25	4.374453193	0.2	0.02	10	0.00252	32	654466	0.2899	0.02314	33.7730251
4446	2.286	4.23	6.7056	1.225	10	10	25	4.374453193	0.2	0.02	10	0.00252	64	654415	0.28831	0.03273	33.58779188
4446	2.286	4.23	6.7056	1.225	10	10	30	4.374453193	0.2	0.02	10	0.00252	10	667377	0.28125	-0.02843	32.76530979
4446	2.286	4.23	6.7056	1.225	15	15	30	6.56167979	0.2	0.02	10	0.00252	16	1113902	0.28459	0.03528	33.15441605
4446	2.286	4.23	6.7056	1.225	15	15	35	6.56167979	0.2	0.02	10	0.00252	16	1257683	0.27402	0.11379	31.92302289
4446	2.286	4.23	6.7056	1.225	20	20	35	8.748906387	0.2	0.02	10	0.00252	16	1679908	0.27927	0.02303	32.53464201
4446	2.286	4.23	6.7056	1.225	25	25	35	10.93613298	0.2	0.02	10	0.00252	16	1679908	0.27847	0.01411	32.44144291
4446	2.286	4.23	6.7056	1.225	30	30	35	13.12335958	0.2	0.02	10	0.00252	16	3241792	0.27425	-0.17717	31.94981764
4446	2.286	4.23	6.7056	1.225	15	15	45	6.56167979	0.2	0.02	10	0.00252	16	1565351	0.27923	-0.12629	32.52998206
4446	2.286	4.104	6.7056	1.225	15	15	45	6.56167979	0.2	0.02	10	0.00252	16	1257684	0.27456	-0.09474	31.03315984
4446	2.286	4.104	6.7056	1.225	15	15	50	6.56167979	0.2	0.02	10	0.00252	16	1724684	0.26671	0.00949	30.14588454
4446	2.286	4.104	12.6	1.225	15	15	50	6.56167979	0.2	0.02	10	0.00252	3	2814195	0.08906	-0.00823	35.54162057
4446	2.286	4.104	12.6	1.225	15	15	50	6.56167979	0.2	0.02	10	0.00252	16	3583715	0.24251	-0.05292	96.77968116
4446	2.286	4.104	12.6	1.225	15	15	50	6.56167979	0.2	0.02	10	0.00252	16	3930502	0.27103	0.09354	108.1613005
4446	2.286	4.104	1.26	1.225	15	15	50	6.56167979	0.2	0.02	10	0.00252	3	2815887	0.28034	0.15858	1.118766889
4446	2.286	4.104	1.26	1.225	15	15	50	6.56167979	0.2	0.02	10	0.00252	16	3194487	0.39251	0.04479	1.56640933
4446	2.286	4.104	1.26	1.225	15	15	50	6.56167979	0.2	0.02	10	0.00252	24	3828386	0.36338	0.00958	1.450158779
4446	2.286	4.104	1.26	1.225	15	15	50	6.56167979	0.2	0.02	10	0.00252	32	4309663	0.38835	-0.0488	1.549807809
M.R.	2.286	4.104	1.26	1.225	15	15	50	6.56167979	0.2	0.02	10	0.00252	32	3827880	0.36254	0.00142	1.446806549
	2.286	4.104	1.26	1.225	15	15	50	6.56167979	0.2	0.02	10	0.00252	32	3827880	0.36254	0.00142	1.446806549

Sphere M	Diame	Front Ar	Velocity	Density	With	Height	Length	W/D ratio	Far Fie	BL heigh	Layers	# of Element	Drag Co	Lift Coef	Drag Force
4446	2.286	4.23	6.7056	1.225	0	0	0	0.00	0	0	0	0	0.1	0	11.649888
4446	2.286	4.23	6.7056	1.225	8	8	45	3.50	0.2	0.00252	5	3125132	0.141	-0.082	16.426342
4446	2.286	4.23	6.7056	1.225	10	10	45	4.37	0.2	0.00252	5	3836256	0.139	-0.084	16.193344
4446	2.286	4.23	6.7056	1.225	12	12	45	5.25	0.2	0.00252	5	5984420	0.135	-0.082	15.727349
4446	2.286	4.23	6.7056	1.225	14	14	45	6.12	0.2	0.00252	5	7861876	0.126	-0.045	14.678859
4446	2.286	4.23	6.7056	1.225	20	20	45	8.75	0.2	0.00252	5	14013971	0.126	-0.063	14.678859
4446	2.286	4.23	6.7056	1.225	26	26	45	11.37	0.2	0.00252	5	25122791	0.124	-0.053	14.445861
4446	2.286	4.23	6.7056	1.225	34	34	45	14.87	0.2	0.00252	5	40663846	0.124	-0.062	14.445861
4446	2.286	4.23	6.7056	1.225	44	44	45	19.25	0.2	0.00252	5	3125132	0.124	-0.01947	14.445861
4446	2.286	4.23	6.7056	1.225	24	24	45	10.50	0.2	0.00252	1	19160724	0.182	-0.016	21.202796
4446	2.286	4.23	6.7056	1.225	24	24	45	10.50	0.2	0.00252	5	19160724	0.126	0.055	14.678859
4446	2.286	4.23	6.7056	1.225	24	24	45	10.50	0.2	0.00252	10	19160724	0.182	-0.016	21.202796
4446	2.286	4.23	6.7056	1.225	24	24	45	10.50	0.2	0.00252	15	19160724	0.182	-0.016	21.202796
4446	2.286	4.23	6.7056	1.225	24	24	45	10.50	0.2	0.00252	20	19160724	0.182	-0.016	21.202796

Simulation Results for Vehicle simulations

Wheels	Rotating	Area	Velocity	Density	Drag Coef	Drag Force	Elem Size	No. Elem
out	No	0.375	6.706	1.225	0.345	3.56	?	1.93E+06
out	No	0.315	6.706	1.225	0.315	2.73	?	1.36E+07
In	No	0.441	6.706	1.225	0.292	3.55	?	6.48E+06
In	No	0.441	6.706	1.225	0.242	2.94	?	8.58E+06
In	yes	0.441	6.706	1.225		0.00	?	
out	no	0.375	6.706	1.225	0.396	4.09	0.4	1.90E+06
out	no	0.375	6.706	1.225	0.334	3.45	0.2	3.71E+06
out	no	0.375	6.706	1.225	0.318	3.28	0.1	1.36E+07
out	no	0.375	6.706	1.225	0.308	3.18	0.05	8.33E+07
in	no	0.441	6.706	1.225	0.557	6.77	0.4	6.40E+06
in	no	0.441	6.706	1.225	0.266	3.23	0.2	8.48E+06
in	no	0.441	6.706	1.225	0.246	2.99	0.1	1.85E+07
in	no	0.441	6.706	1.225	0.236	2.87	0.05	8.81E+07
out	yes	0.375	6.706	1.225	0.336	3.47	0.4	1.90E+06
out	yes	0.375	6.706	1.225	0.278	2.87	0.2	3.70E+06
out	yes	0.375	6.706	1.225	0.272	2.81	0.1	1.36E+07
in	yes	0.441	6.706	1.225	0.511	6.21	0.4	6.40E+06
In	yes	0.441	6.706	1.225	0.253	3.07	0.2	8.79E+06
In	yes	0.441	6.706	1.225	0.226	2.75	0.1	1.84E+07

Vehicle Height Simulation Results

Vehicle Height	Element size	# of Elemnts	Drag Coef	Lift Coef	Frontal Area	Drag Force	H/L
4.50	0.05	8.33E+07	0.309	0.145	0.375	3.191706429	0.046875
3.95	0.4	1907107	0.382	0.073	0.369	3.882602415	0.041146
3.95	0.2	3723767	0.323	0.112	0.369	3.282933455	0.041146
3.95	0.1	13609698	0.317	0.123	0.369	3.221950171	0.041146
3.95	0.05	83312169	0.312	0.139	0.369	3.171130768	0.041146
3.40	0.4	2566611	0.317	0.124	0.36	3.143366021	0.035417
3.40	0.2	4277500	0.316	0.129	0.36	3.13345004	0.035417
3.40	0.1	13720619	0.322	0.124	0.36	3.192945926	0.035417
3.40	0.05	83350577	0.319	0.137	0.36	3.163197983	0.035417
2.85	0.4	1922406	0.493	0.054	0.353	4.793523004	0.029688
2.85	0.2	3735339	0.339	0.142	0.353	3.296154763	0.029688
2.85	0.1	13606764	0.325	0.132	0.353	3.160030378	0.029688
2.85	0.05	83308624	0.321	0.153	0.353	3.121137696	0.029688
2.30	0.4	1873725	0.508	0.045	0.346	4.841422702	0.023958
2.30	0.2	3696305	0.34	0.13	0.346	3.240322281	0.023958
2.30	0.1	13567111	0.329	0.121	0.346	3.135488325	0.023958
2.30	0.05	83261017	0.322	0.142	0.346	3.068775807	0.023958
1.75	0.4	2727375	0.324	0.105	0.338	3.016441462	0.018229
1.75	0.2	4441571	0.324	0.102	0.338	3.016441462	0.018229
1.75	0.1	13907607	0.329	0.095	0.338	3.062991485	0.018229
1.75	0.05	83529649	0.325	0.103	0.338	3.025751467	0.018229

Curriculum Vita

Christian A. Mata has a Bachelor's Degree in Mechanical Engineering from the University of Texas at El Paso (UTEP). He has 4 years of experience working with the design and development of the Shell Eco-Marathon competition prototype vehicle for UTEP. While working on this project he has been involved with every aspect of the vehicle including powertrain design, fuel delivery systems, as well as steering mechanism design. Christian continued his studies at UTEP in order to pursuit a master of science degree in mechanical engineering. While working towards this master's degree, he was also working as a research assistant in the University of Texas at El Paso: Lockheed Martin Lab. Where he gained experienced in wind tunnel testing as well as 3D printing and rapid prototyping. During this time, he was also appointed as an undergraduate instructor. This involved teaching a course involving the optimization of designs for different manufacturing methods, as well as geometric dimensioning and tolerancing. While working on this research, he did a large amount of work with high power computing. His knowledge of computational fluids was then focused on the application of aerodynamics.

Permanent address: 208 Colorado Dr.
Sunland Park, New Mexico, 88063

This thesis/dissertation was typed by Christian A. Mata.